

Instituto Tecnológico de Costa Rica
(Costa Rica Institute of Technology)

Electronic Engineering Department

TEC | Tecnológico
de Costa Rica

TUHH

Technische Universität Hamburg

Institute of Electromagnetic Theory

Hamburg-Harburg University of Technology

**“Whole-Body SAR simulations on a prolate spheroid
using different plane wave polarizations up to 100 GHz”**

Project Submitted in Partial Fulfillment of the
Requirements for the Degree *Licenciatura en Ingeniería Electrónica*

José Enrique Hernández Bonilla

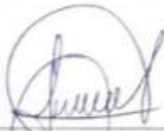
27/02/2018

INSTITUTO TECNOLÓGICO DE COSTA RICA
ESCUELA DE INGENIERÍA ELECTRÓNICA
PROYECTO DE GRADUACIÓN
ACTA DE APROBACIÓN

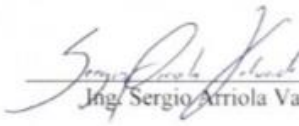
Defensa de Proyecto de Graduación
Requisito para optar por el título de Ingeniero en Electrónica
Grado Académico de Licenciatura
Instituto Tecnológico de Costa Rica

El Tribunal Evaluador aprueba la defensa del proyecto de graduación denominado "Whole-Body SAR simulations on a prolate spheroid using different plane wave polarizations up to 100 GHz", realizado por el señor José Enrique Hernández Bonilla y, hace constar que cumple con las normas establecidas por la Escuela de Ingeniería Electrónica del Instituto Tecnológico de Costa Rica.

Miembros del Tribunal Evaluador



Ing. Anibal Coto Cortés
Profesor lector



Ing. Sergio Arriola Valverde
Profesor lector



Ing. Renato Rimolo Donadio
Profesor asesor

Cartago, 27 de febrero de 2018

Declaración de autenticidad

Declaro que el presente Proyecto de Graduación ha sido realizado, en su totalidad, por mi persona, utilizando y aplicando literatura referente al tema e introduciendo conocimientos propios.

En los casos en que he utilizado material bibliográfico, he procedido a indicar las fuentes mediante citas.

En consecuencia, asumo la responsabilidad total por el trabajo de graduación realizado y por el contenido del correspondiente informe final.



José Enrique Hernández Bonilla

Cédula: 1-1602-0184

Abstract

A study on specific absorption rate (SAR) measurements using computational tools is presented. Using various numerical tools, ranging from full-wave simulators to physical optics, a prolate spheroid is irradiated by different polarized plane waves in the frequency range of 10 MHz - 100 GHz. For the low frequency range full-wave simulators were used to obtain the whole-body SAR of the prolate spheroid. When technical limitations were reached by this methodology, a physical optics approach was used to reach whole-body SAR measurements to a 100 GHz. As a side study, the electrical properties of water were studied with the goal of using them in both approaches. This project is a joint effort between the Technical University of Hamburg (TUHH) and the Technical Institute of Technology of Costa Rica (TEC).

Keywords: Computational Electromagnetics, Material Electrical Properties, Physical Optics, SAR.

*To my Family and my Friends,
Who have always supported me*

Acknowledgement

First and foremost, to my advisor Dr-Ing. Renato Rímolo Donadio, without him this project would have never happened; his support and guidance were crucial for the completion of this work. I thank him for his confidence on my abilities over these years.

To the professors, Dr. sc. techn. Christian Schuster and Dr.-Ing. Heinz-D. Brüns for all the support given to me while I was working with them. For always asking how I was feeling and giving me the necessary feedback to move forward in my work.

To all the staff at TET-TUHH who always tried to make me feel part of them. For that I am very grateful and hope we can see each other somewhere in the future. You made my first experience abroad a most welcoming one.

To my friends, thank you for making these years a thrill ride. The laughs, stress and fun we've had throughout these years I won't change them for nothing. You have also been a powerful pillar in this journey and I hope we can still be in each other's life for years to come.

To my girlfriend Daniela, without you and your unconditional support I would have probably never made it. Thanks for being a powerful force in my life, you've made a better person all around. This is for you.

Finally, to my family, without their unconditional love and support I would have never been able to achieve all my goals through my academic years. I thank them for always believing in me and giving me the tools to work these 5 years. This project is for them.

José Enrique Hernández

February 27, 2018

INDEX

1. Introduction	1
2. Fundamental Information	4
2.1 Electromagnetics Fundamentals	4
2.2 Plane Wave Polarizations	5
2.3 Electrical Properties of Lossy Materials	7
2.4 EM Dosimetry	9
2.5 Case of Study: Prolate spheroid irradiated by a plane wave	10
3. SAR computations at High Frequencies	14
4. Whole-body SAR on a prolate spheroid using full-wave simulators	16
4.1 Simulation Setup	16
4.1.1 Modeling of a prolate spheroid using CST	17
4.1.2 Modeling of a prolate spheroid using CONCEPT-II	22
4.2 Whole-body SAR on a prolate spheroid using full-wave simulators CST and CONCEPT-II	24
4.2.1 EHK Polarization	25
4.2.2 HEK Polarization	29
4.2.3 KEH Polarization	31
4.2.4 Whole-body SAR, final comparisons and other simulations	33
4.3 Computational limitations on full-wave simulations	35
5. Influence of material selection on EM radiation problems	38
5.2 Perpendicular incidence of a plane wave on a water surface	38
5.2.1 Frequency Independent Material (FIM) Model of Water	39
5.2.2 Frequency Dependent Material (FDM) Model of Water	43
5.3 General incidence of a plane wave on a water surface	47
5.3.1 Frequency Independent Material (FIM) Model of Water	48
5.3.2 Frequency Dependent Material (FDM) Model of Water	49
5.4 Skin Depth of Water	50
6. Whole-body SAR on a prolate spheroid using physical optics for very high frequencies	51
6.2 EHK Polarization	54
6.3 HEK Polarization	56

6.4	KEH Polarization.....	58
6.5	Full spectrum of whole-body SAR in terms on different wave polarizations	60
7.	Conclusions.....	62
8.	Recommendations	64
9.	References	65

FIGURE INDEX

Figure 1.	Prolate spheroid irradiated by a plane wave.	2
Figure 2.	Different wave polarizations for a prolate spheroid. Taken from [21].	6
Figure 3.	Different wave polarizations for an ellipsoid. Taken from [21].	7
Figure 4.	Problem of interest: Prolate spheroid radiated with a plane wave. Taken from [21].	10
Figure 5.	Average whole-body SAR as a function of frequency for models of an average man in free space for three polarizations, E, H, and K. The incident wave is a planewave with a power density of 1 mW/cm ²	12
Figure 6.	Prolate Spheroid Specifications.	18
Figure 7.	Plane wave specifications window in CST.....	19
Figure 8.	Mesh properties window in CST.....	19
Figure 9.	Symmetry planes window in CST.	20
Figure 10.	Monitor set up window in CST.....	21
Figure 11.	Results tab in CST.	21
Figure 12.	CAD tool for geometry modeling in CONCEPT-II.....	22
Figure 13.	Plane wave description window in CONCEPT-II.	23
Figure 14.	Whole-body SAR for E Polarization on CST and CONCEPT-II.	25
Figure 15.	Whole-body SAR with different mesh density for E Polarization from 10 MHz to 100 MHz.....	28
Figure 16.	Whole-body SAR with different mesh density for E Polarization from 1 GHz to 2 GHz.....	28
Figure 17.	Whole-body SAR for H Polarization on CST and CONCEPT-II.....	29
Figure 18.	Whole-body SAR for H Polarization on CST and CONCEPT-II.....	31
Figure 19.	Whole-body SAR for 3 Polarizations in CST.....	33
Figure 20.	Whole-body SAR for 3 Polarizations in CONCEPT-II.....	33
Figure 21.	Whole-body SAR for 3 different size prolate spheroids in CST.	34
Figure 22.	Whole-body SAR for 3 different size prolate spheroids in CONCEPT-II.	34
Figure 23.	1D Perpendicular incidence model.....	39
Figure 24.	Water electric permittivity values for a FIM model.....	40
Figure 25.	Attenuation and phase constant values for a FIM model.....	41
Figure 26.	Wave impedance values for a FIM model.	41
Figure 27.	Reflection coefficient values for a FIM model.	42

Figure 28. Transmission coefficient values for a FIM model.	42
Figure 29. Water electric permittivity values for a FDM model.	44
Figure 30. Attenuation and phase constant values for a FDM model.	44
Figure 31. Wave impedance values for a FDM model.	45
Figure 32. Reflection coefficient values for a FDM model.	46
Figure 33. Transmission coefficient values for a FDM model.	46
Figure 34. 1D General incidence model.	47
Figure 35. Reflection coefficient values for a FIM model with different angles on incidence.	48
Figure 36. Transmission coefficient values for a FIM model with different angles on incidence.	49
Figure 37. Reflection coefficient values for a FDM model with different angles on incidence.	49
Figure 38. Transmission coefficient values for a FDM model with different angles on incidence.	50
Figure 39. Definition of incident angle alpha for the incident wave.	52
Figure 40. Whole-body SAR for E polarization up to 100 GHz using a FIM model.	54
Figure 41. Whole-body SAR for E polarization up to 100 GHz using a FDM model.	55
Figure 42. FDM Model vs FIM Model for E polarization.	55
Figure 43. Whole-body SAR for H polarization up to 100 GHz using a FIM model.	56
Figure 44. Whole-body SAR for H polarization up to 100 GHz using a FDM model.	57
Figure 45. FDM Model vs FIM Model for H polarization.	57
Figure 46. Whole-body SAR for K polarization up to 100 GHz using a FIM model.	59
Figure 47. Whole-body SAR for K polarization up to 100 GHz using a FDM model.	59
Figure 48. FDM Model vs FIM Model for K polarization.	60
Figure 49. Whole-body SAR for 3 polarizations up to 100 GHz using a FIM model.	61
Figure 50. Whole-body SAR for 3 polarizations up to 100 GHz using a FDM model.	61

TABLE INDEX

Table 1. Parameters for the model of interest.	11
Table 2. Effects of Polarization in Whole-body SAR measurements. Taken from [21].	13
Table 3. State of the art for SAR computations.	14
Table 4. Simulation Parameters.	17
Table 5. Polarization Parameters for plane wave in CST.	18
Table 6. Symmetry parameters used in figure 8.	20
Table 7. Angle values for different polarizations on CONCEPT-II.	24
Table 8. CST model information for the calculation of whole-body SAR in E polarization.	26
Table 9. CONCEPT-II model information for the calculation of whole-body SAR in E polarization.	27
Table 10. CST model information for the calculation of whole-body SAR in H polarization.	30
Table 11. CONCEPT-II model information for the calculation of whole-body SAR in H polarization.	30

Table 12. CST model information for the calculation of whole-body SAR in K polarization.	32
Table 13. CONCEPT-II model information for the calculation of whole-body SAR in K polarization.	32
Table 14. Mesh cells in CST using 10 basis functions per wavelength.....	35
Table 15. Memory needed to perform prolate spheroid simulations using a model with 10 basis functions per wavelength.	36
Table 16. Memory required for running simulations in CONCEPT-II for a prolate spheroid with optimized mesh for E and K polarizations.	37
Table 17. Skin depth for FDM Model and FIM Model.	50

1. Introduction

In recent years there has been an increase in the quantity of electronic devices that require the use of some form of Electromagnetic (EM) radiation to work. While some are used on industrial applications, there is a vast quantity that is present in our daily activities. From cellphones to WiFi routers, we are in constant interaction with EM fields, for this reason there is a necessity of studying the effects caused by the interaction between them and our bodies.

This field of study is known as Bioelectromagnetics and one of the mayor interests of research is the interaction between the EM radiation and the different tissues of our body. One of the methods used for this application is the measurement of the specific absorption rate (SAR) which is a very important metric that helps us understand some of the effects of EM radiation on our bodies. With SAR, guidelines have been developed for the public health in terms of allowed exposure to EM fields from devices like cellphones or telecommunication antennas.

Due to ethical and practical reasons, most of the research is conducted via computer simulations using different numerical methods to calculate the interaction between EM fields and biological tissues. Most of the research studies work in frequencies lower than 10 GHz because most of the applications of interest are in this region; but with the advent of new technologies that work on frequencies higher than 10 GHz, there is a need for new SAR studies to understand how these new technologies will affect us. This leaves us with a question: How far in frequency can we reach using different EM simulations to obtain valid measurements of the interactions between EM fields and biological tissues?

This report presents a study on the current state of EM simulations for a classical problem of Bioelectromagnetics. The problem consists on the use of a plane wave as a source of EM energy radiating on a prolate spheroid made of water or other

material using three different wave polarizations. The purpose of this problem is to study the Whole-body SAR on the body using the different polarizations.

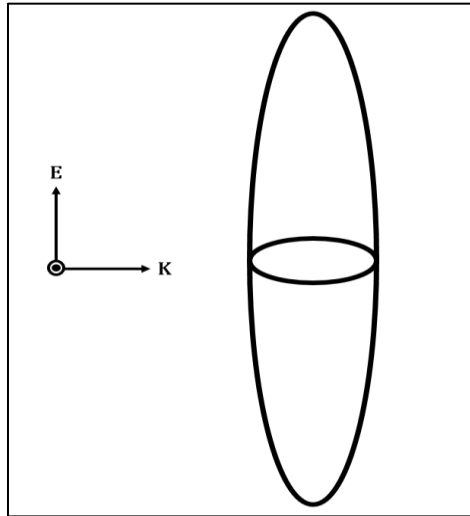


Figure 1. Prolate spheroid irradiated by a plane wave.

The main objective of this project is to analyze the performance of full-wave simulators to tackle complex Bioelectromagnetics problems in high frequencies and to develop a methodology to achieve simulations up to a 100 GHz. Simulations will be performed using full-wave simulators up to the computational resources available start to fail, then a different approach using physical optics will be used to expand on the range of the first simulations.

This work is divided in 6 chapters. Chapter 2 covers the fundamentals of electromagnetic theory needed to understand the different measurements and simulations of the report. From Maxwell equations to EM dosimetry, the idea is to give a basic understanding of the topics treated.

Chapter 3 covers the state of the art in terms of SAR computations, giving insight in techniques and models used, also frequencies achieved and the specific SAR computations that were performed by each research.

Chapter 4 covers the calculation of whole-body SAR in a prolate spheroid using different full-wave simulators. Technical limitations are presented for each simulator and comparisons between solvers are shown.

Chapter 5 covers a study of the electrical properties of materials using a 1D approach based on a one dimensional transmitted wave against a vertical surface. The effects of the angle of incidence of the wave on the material and the modeling of the material are studied and compared between each other.

Finally, chapter 6 covers the development of a methodology to analyze the whole-body SAR on a prolate spheroid for frequencies higher than 10 GHz using physical optics. Comparisons between full-wave simulations results from chapter 2 are made and a full picture of the whole-body SAR on frequency is presented.

This report is a joint project at the Technical University of Hamburg (TUHH) with the Costa Rica Institute of Technology (TEC).

2. Fundamental Information

2.1 Electromagnetics Fundamentals

The study of electromagnetic radiation is possible thanks to Maxwell's Equations; this system of equations helps us to understand the propagation of electromagnetic radiation in its entire spectrum. Unfortunately, this set of equations can only solve a handful of problems analytically due to the complexity of its solutions. For this reason, in practice, the use of numerical tools is favored to solve complex problems of electromagnetics which is the basis of the field known as Computational Electromagnetics (CEM).

When structures cannot be treated as lumped elements anymore, the use of CEM is fundamental to understand the behavior of electromagnetic radiation. With different methods, each one with its advantages and disadvantages, Maxwell's Equations are discretized and used to find solutions to different problems.

$$\oint \vec{D} \cdot d\vec{S} = \int_V \rho_v dV \quad (1) \quad \nabla \cdot \vec{D}(\vec{r}, t) = \rho_v(\vec{r}, t) \quad (5)$$

$$\oint \vec{E} \cdot d\vec{L} = -\frac{d}{dt} \int_V \vec{B} \cdot d\vec{S} \quad (2) \quad \nabla \times \vec{E}(\vec{r}, t) = -\frac{\partial \vec{B}(\vec{r}, t)}{\partial t} \quad (6)$$

$$\oint \vec{B} \cdot d\vec{S} = 0 \quad (3) \quad \nabla \cdot \vec{B}(\vec{r}, t) = 0 \quad (7)$$

$$\oint \vec{H} \cdot d\vec{L} = I + \int_V \frac{\partial \vec{D}}{\partial t} \cdot d\vec{S} \quad (4) \quad \nabla \times \vec{H}(\vec{r}, t) = \vec{J}(\vec{r}, t) + \frac{\partial \vec{D}(\vec{r}, t)}{\partial t} \quad (8)$$

The scope of this report is to solve a classic problem of Bioelectromagnetics, which due to its complexity needs the use of CEM to obtain solutions via computer simulations. The methods of CEM used in this report to solve this problem are the Finite Integration Technique (FIT) and the Method of Moments (MoM).

2.2 Plane Wave Polarizations

When working with EM simulations; most of the time, there will be the need of setting up a source of electromagnetic radiation; be it an antenna, a waveguide, a voltage source or a plane wave. Sources can be the object of study of the simulation or the incident energy on the body of study. In Bioelectromagnetics, the interest is to simulate the interaction between electromagnetic radiation and biological tissues, so most of the time sources will be used as field generators that will interact with the body or tissue of interest.

When working with full human body models, a plane wave may be preferred due to the simplicity of its formulation in comparison to that of an antenna, saving time in the simulation duration. The orientation of the incident E and H Fields of the plane wave with respect to these irradiated models has a very strong effect on the strength of the fields inside the body. [1]

Depending on the object used, there will be different wave polarizations that can be used to irradiate it and obtain different measurements. For objects with circular symmetry in the long axis like prolate spheroids; three polarizations are defined:

- E Polarization → Electric Field is parallel to the long axis.
- H Polarization → Magnetic Field is parallel to the long axis.
- K Polarization → Propagation Vector is parallel to the long axis.

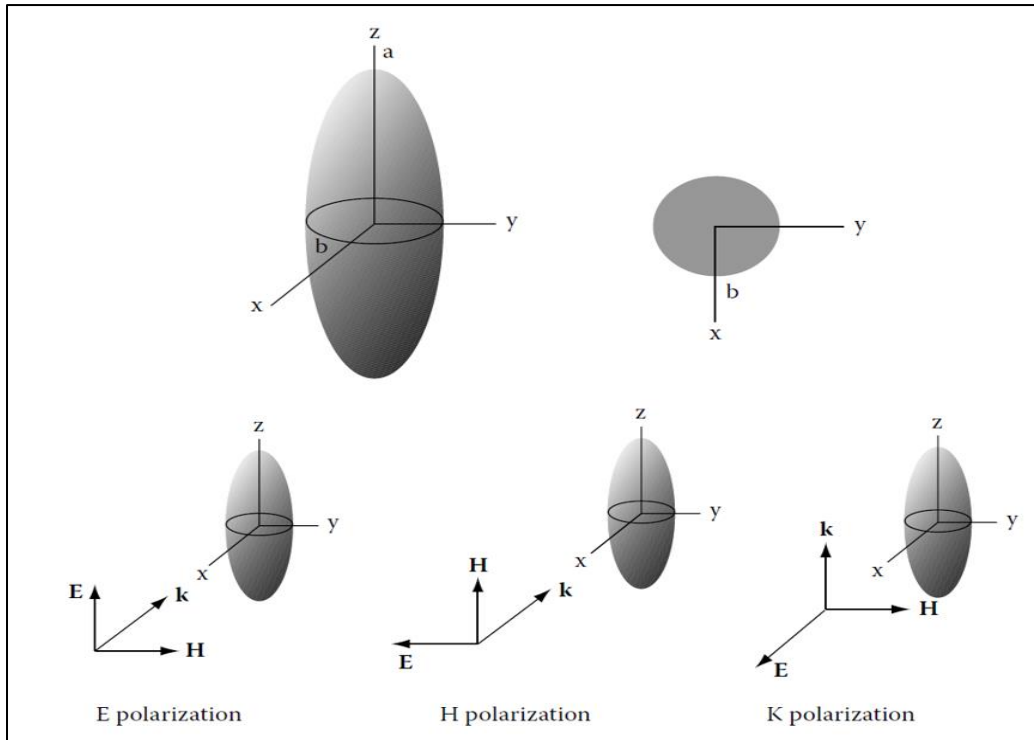


Figure 2. Different wave polarizations for a prolate spheroid. Taken from [21].

Human body models are very complex geometrically and don't have circular symmetry about their long axis, for this reason ellipsoids can be used as a rough approximation. In the case of an ellipsoid 6 polarizations are defined based on its 3 axes.

As mentioned before, orientation plays a big part on the strength of the inside fields generated by a plane wave. This happens because the cross-sections where the incident fields radiate are different for each polarization and in some scenarios, like K polarizations, the waves have to travel a longer distance through the body which also varies the overall effect of the energy absorbed by the body.

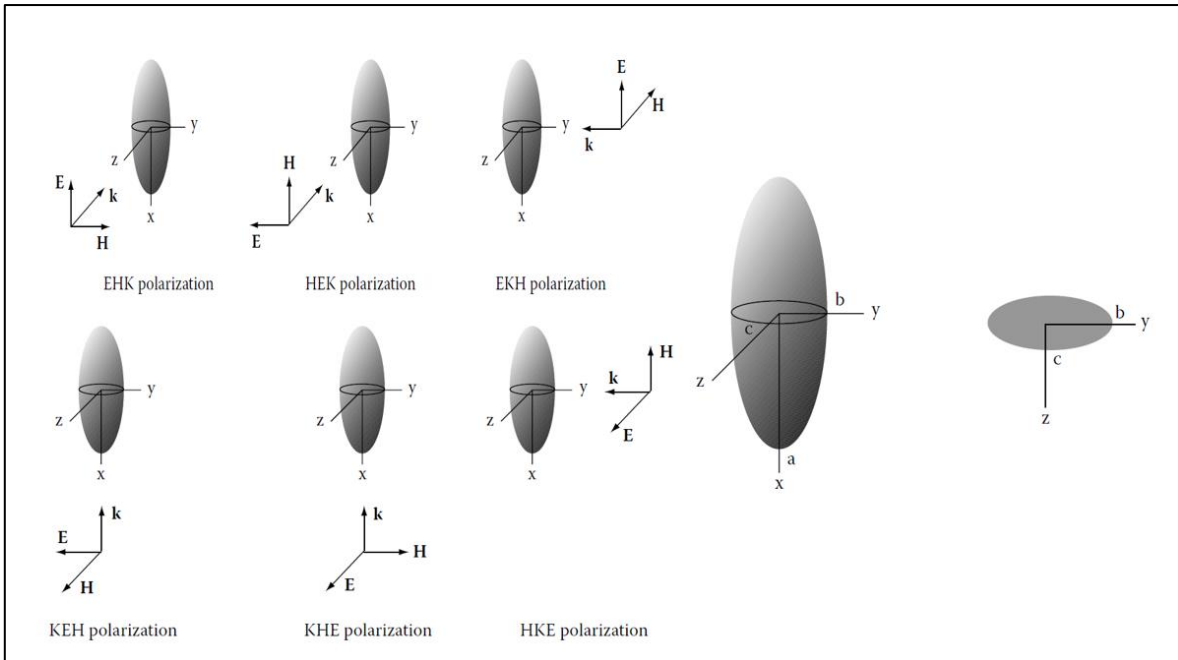


Figure 3. Different wave polarizations for an ellipsoid. Taken from [21].

2.3 Electrical Properties of Lossy Materials

Electromagnetic radiation behaves differently when interacting with materials, whether they are lossless or lossy. A good way to understand this behavior is using the plane wave equations to explain the different effects present. In Bioelectromagnetics, tissues are normally lossy and frequency dependent, which makes this analysis necessary to understand the effects of radiation and how internal fields will behave in a body. Because the focus of this report is in Bioelectromagnetics, this section will be focused on lossy material behavior.

When we talk about lossy medium, we are stating that they have a certain conductivity σ which generates the losses on the medium. In biological tissues losses appear due to the complex permittivity of the tissue. This means that for a wave propagating in a lossy material, the propagation constant turns complex and must be defined as:

$$\gamma = \alpha + j\beta = j\omega\sqrt{\mu\varepsilon}\sqrt{1 - j\frac{\sigma}{\omega\varepsilon}} \quad (9)$$

If we solve the plane wave equation with this complex propagation constant, for a wave travelling in the +z direction, we end with the following equation [22]

$$\vec{E} = E e^{-\alpha z} \cos(\omega t - \beta z) \quad (10)$$

Where α is the attenuation constant which serves as a damping factor and β is the phase constant which if $\alpha = 0$, $\beta=k$ the wave number for a lossless material. Losses can also be treated through the use of complex permittivity. If $\sigma= 0$ but $\epsilon = \epsilon' - j \epsilon''$, the propagation constant is defined as

$$\gamma = j\omega\sqrt{\mu\epsilon} = j\omega\sqrt{\mu\epsilon'(1 - j \tan \delta)} \quad (11)$$

Where $\tan\delta = \epsilon''/\epsilon''$ is the loss tangent of the material [22].

With some algebra the attenuation and phase constants can be defined as:

$$\alpha = Re\{\gamma\} = \omega \sqrt{\frac{\mu\epsilon'}{2}} \left[\sqrt{1 + \left(\frac{\epsilon''}{\epsilon'}\right)^2} - 1 \right] \quad (12)$$

$$\beta = Im\{\gamma\} = \omega \sqrt{\frac{\mu\epsilon'}{2}} \left[\sqrt{1 + \left(\frac{\epsilon''}{\epsilon'}\right)^2} + 1 \right] \quad (23)$$

Another important quantity for analysis is wave impedance. In vacuum wave impedance is defined as:

$$\eta = \sqrt{\mu_0/\epsilon_0} \quad (34)$$

But in lossy materials the relation between electric and magnetic fields is defined as:

$$\eta = j\omega\mu/\gamma \quad (45)$$

One last important metric to calculate when making Bioelectromagnetic simulations is the skin depth which is derived from the attenuation constant and can be simplified if the material behaves as a good conductor; the window where the assumption of a good conductor can be made depends on the material chosen for the simulation. Skin depth is defined generally as:

$$\delta_s = \frac{1}{\alpha} [m] \quad (56)$$

2.4 EM Dosimetry

In Bioelectromagnetics problems, SAR is a valuable metric that helps us represent the power deposition in the body. As power is proportional to the field strength is important to mention that one characteristic of biological tissue is that it is mostly nonmagnetic, which makes the effect of **H** fields non prominent on EM biological interactions and thus power depends in almost all its totality in the strength of the electric field. SAR is defined as transferred power divided by the mass of the object [21]. It can be represented in different ways but for a time-average the formula is given by:

$$SAR = \frac{\sigma_{eff} E^2}{2\rho} [W/Kg] \quad (17)$$

Where ρ is the density of the material. This relation is punctual because only applies at the given point where **E** has that particular value. For a full approximation of how much power is transferred to a whole-body, the following formula is also useful.

$$SAR_{Whole-Body} = \frac{P_{loss}}{M_{body}} [W/Kg] \quad (18)$$

Where P_{loss} is the power absorbed by the body of interest and M_{body} is the mass of the body.

2.5 Case of Study: Prolate spheroid irradiated by a plane wave

There has been a lot of research regarding the effects of electromagnetic radiation in our bodies. Most of it related to the effects of specific devices and a few about the general effects of radiation. One of the cornerstones in terms of SAR computations is [1]. This research helped to the understanding of electromagnetic dosimetry for humans using whole-body SAR as a metric of how much absorption our bodies receive from EM radiation. Apart from some other investigations, like [7], there has not been an updated revision of this research in terms of newer methods for solving the fields.

For this project the problem of interest is the one developed on [1], which is a prolate spheroid radiated with a plane wave using different wave polarizations. The idea is to obtain the whole-body SAR of this body in three orientations; E, H and K polarization. Originally, this problem was solved using different numerical approximations depending on the frequency range.

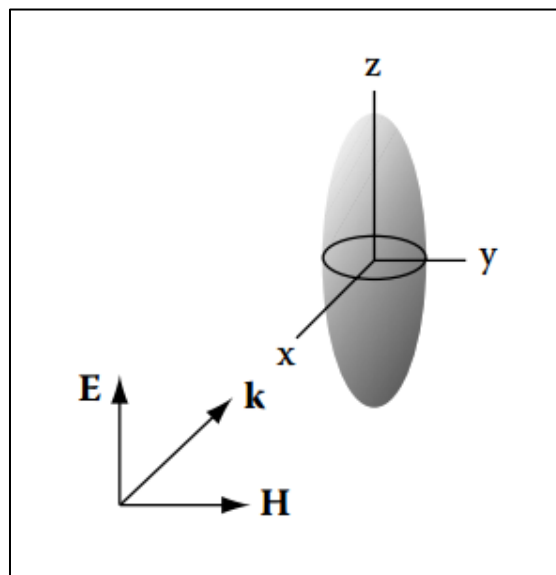


Figure 4. Problem of interest: Prolate spheroid radiated with a plane wave. Taken from [21].

In this report the same problem is tackled using full-wave simulators to obtain similar results as [1]. The idea is to test the capabilities of nowadays hardware and software to run this simulation and see if it can achieve the same frequency range obtained with more archaic methods. If the full-wave simulators start to fail, other approaches will be used to solve the problem. Also a study of the material will be conducted to understand how it affects the overall effects of EM radiation on the body. In terms of the values used for the original problem and the one developed here, there are some punctual differences shown on table 1.

Table 1. Parameters for the model of interest.

	Durney [1]	This Report
a (m)	0.875	0.9
b (m)	0.138	0.15
ϵ_r	42.81	78
σ_{eff} (S/m)	0.6463	1.59
Power Density (mW/cm²)	1	1

Where **a** is the major axis of the prolate spheroid and **b** the minor axis. The materials are 2/3 of muscle for [1] and fresh water for this report. As specified in 2.1, simulations will be run using FIT and MoM. The results expected from the simulations are based on the results from [1] and [7]. For FIT the software of choice is the commercially available software Computer Simulation Technology (CST) Microwave Studio and for MoM, the software used an in-house solver developed by TUHH called CONCEPT-II.

The expected results tells us that for every polarization, the whole-body SAR will behave differently and that every scenario has its own characteristics. The expected behavior can be seen in figure 5, which was obtained from [1].

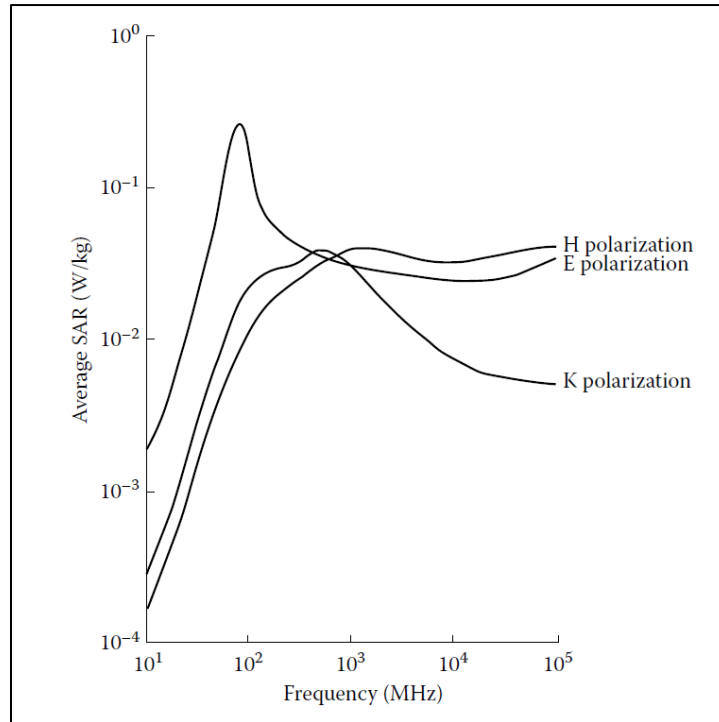


Figure 5. Average whole-body SAR as a function of frequency for models of an average man in free space for three polarizations, E, H, and K. The incident wave is a planewave with a power density of 1 mW/cm².

The calculations shown in the figure are the results of early work using a combination of simple models (prolate spheroid, cylinder, capped cylinder), empirical techniques, and for part of the graph, interpolated estimations [21].

The power absorption can be divided in four regions across the frequency plane. These regions are specific for the E polarization due to the resonance peak present at lower frequencies and were obtained from [7]. The first one is called the sub-resonance region, which goes until 30 MHz and has the characteristic of the body absorption increasing rapidly with a factor of f^2 for all 3 polarizations.

Next is the resonance region, which spans from 30-300 MHz, even though H and K polarizations also reach a peak resonance value, they are not as high as the one obtained by E polarization. This resonance can be compared to that of a wire antenna with the difference that resonance for a biological tissue reaches its peak when the object length is about four-tenths of a wavelength whereas the antenna

has it at when its size is half of the wavelength. The differences are due to the lower conductivity of biological tissues and their size.

The frequency of resonance also depends on the size of the object, in the case of prolate spheroids is closely related to the ratio between the major and the minor axis. If the dimensions are small, like the ones of a small child, the peak of resonance will shift to a higher frequency while if the dimensions are big it will go to a lower frequency [8], also when the resonance peak is passed the whole-body SAR decreases with a factor of approximately $1/f$.

The following is the “Hot-Spots” region; this is due to the absorption being localized in some areas. It spans from 300 MHz to 3 GHz. As seen from figure 5, the whole-body absorption decreases. The final region goes from 3 GHz onwards and it is called the surface absorption region because all the energy absorbed is localized at the surface tissue of the body [7].

At frequencies below resonance, the SAR for E polarization is highest, for H polarization is lowest, and for K polarization is in between the other two. These behaviors are related to the strengths of the internal fields; for example, the internal **E** field is stronger when the incident **E** field is parallel to the body of interest than when it is normal to the surface. Also, the internal **E** field generated from the incident **H** field is greater when the cross-sectional area intercepted is big [21]. In table 2, a summary of these behaviors is made.

Table 2. Effects of Polarization in Whole-body SAR measurements. Taken from [21].

Polarization	E_{inc}	H_{inc}	E_{Eint}	E_{Hint}	Relative SAR
E	Mostly parallel	Intercepts large cross section	Strong	Strong	Highest
K	Mostly normal	Intercepts large cross section	Weak	Strong	Middle
H	Mostly normal	Intercepts small cross section	Weak	Weak	Lowest

3. SAR computations at High Frequencies

To get a better understanding on why it is important to study the effects of electromagnetic radiation, table 3 shows what has been done for SAR computations in terms of simulation performed, models, numerical solvers, frequency ranges and excitations.

Table 3. State of the art for SAR computations.

Reference	Model	Excitation	Min. Freq. (MHz)	Max. Freq. (MHz)	SAR Measurement	Solver
[1]	Ellipsoid and Spheroid	Analytical Solution	10	100000	Average	-
[2]	MRI male volunteer voxel	Plane Wave in horizontal and vertical polarization	600	6000	Average	In-house FDTD
[3]	Human Volunteers	Plane Wave in E polarization	7	40.68	Whole-body	-
[4]	Heterogeneous body model	Plane Wave in vertical polarization	10	900	Whole-body Local	In-house FDTD
[5]	Ellipsoid	Analytical Solution	-	0.00005	Electric Fields Magnetic Fields	-
[6]	Ellipsoid	Plane Wave in E polarization	10	500	Whole-body	CST (FIT)
[7]	Ellipsoid	Plane Wave in E, H, K polarization	10	2450	Whole-body	CST (FIT)
[8]	Pregnant woman voxel model	Plane Wave AP and LR	10	2000	Whole-body Average	In-house FDTD
[9]	Visible Human (VH) model and Ellipsoid	Plane Wave in horizontal and vertical polarization	-	2100	Whole-body Local	In-house FDTD
[10]	SAM Phantom	60 GHz Antenna	-	60000	Peak	CST (FIT)
[11]	Voxel Model	Dipole Antenna	-	1750	No specify	In-house FDTD
[12]	Multi-Layer Model	Dipole Antenna	-	900	Point SAR	CST (FIT)
[13]	Voxel model from University of Florida	Plane Wave in E polarization	50	4000	Whole-body	In-house FDTD
[14]	Realistic 3D human head and shoulders mesh, developed from NMR	Vertically polarized, half-wave thin wire dipole	900	1800	Whole-Head Local Peak	XFDTD
[15]	Scaled adult voxel model	Plane Wave AP and LR	30	3000	Whole-body Average	In-house FDTD
[16]	Phantom from University of Utah	Plane Wave in E polarization	600	3000	Average	In-house FDTD
[17]	Sphere and Ellipsoid	Plane Wave in E polarization	1000	Sphere 10000 SE 10000 LS 3000	Electric Fields	HFSS (FEM) CONCEPT (MoM) CST (FIT)
[18]	Layered planar tissue model VH model	Dipole Antenna	300	6000	Average Local	SEMCAD-X (FDTD)
[19]	SEMCAD Phantom Model	Monopole-helix Monopole	-	1800	No specify	SEMCAD-X (FDTD)
[20]	SAM Phantom	Monopole	938	1818	No specify	CST (FIT)

*Note: For [17] SE: Small Ellipsoid / LS: Large Ellipsoid

In table 3, we can see that most of the research has used geometrical models [1] [5] [6] [7] [17] or complex 3D human models [8]-[11], [13]-[16], [19]-[20]. There is also a preference for using the Finite-Difference Time Domain Method (FDTD) to solve most of these simulations, this is partly due to the “simplicity” associated with the implementation of this method, which makes it easy to be implemented “in house”. Others use commercial software like CST or SEMCAD-X.

Finally, there is an important trend. Most of the studies that use a numerical method provide results for frequencies minor to 10 GHz. Only a handful of references ([1], [10]) performed studies beyond this frequency; this could mean that most of the research has been made with the current operating frequency of RF devices in mind, leaving a whole part of the spectrum without serious research.

4. Whole-body SAR on a prolate spheroid using full-wave simulators

4.1 Simulation Setup

To set these simulations, there are a lot of parameters that need to be considered. For example, the reason why a simpler geometry is chosen for the simulations is due to the complexity of 3D models of human bodies for full-wave simulations. The prolate spheroid is a relatively good and simple model to calculate the effects of different wave polarizations on the human body. It's important to remember that this model only provides an intuitive understanding of the behavior of the electromagnetic fields on the human body as they would only be accurate if the human body were shaped like a prolate spheroid [21].

Prolate spheroids have a mayor axis and one minor axis. The mayor axis helps to represent the height of the body of interest and the minor one helps to describe the width of the model. They also have the advantage of having symmetry, not only in the geometrical sense but in the electrical one, which can optimize the solution time and reach of the simulations. For the scope of this work, the model was obtained using the modelling tools of CST and CONCEPT-II.

The model dimensions, as seen from table 1, for the simulations are a height of 1.8 meters and a width of 0.3 meters, which corresponds to an approximation of an adult male. It is also important to remember that due to the model geometrical symmetry there will be no real differences between some polarizations as EHK and EKH, HEK and HKE, and, KHE and KEH which simplifies even further the number of simulations needed. For this reason, the polarizations used for the simulations will be EHK, HEK and KEH.

Finally, table 4 gives a summary of all the important parameter needed to run the simulations smoothly. With all these parameters we can obtain the values for whole-body SAR for the prolate spheroid up to high frequencies.

Table 4. Simulation Parameters.

	Parameter	Value
Source	Power Density	1 [mW/cm ²]
	Excitation	Plane Wave
Material	ϵ_r	78
	Conductivity	1,59 [S/m]
Geometry	Height	1.8 m
	Width	0.3 m

4.1.1 Modeling of a prolate spheroid using CST

To model a prolate spheroid on CST the following steps must be followed. On the *Modeling* tab, the following icon must be used . The option Analytical Face helps to model more complex geometries like a prolate spheroid. In figure 5, the information needed to model the spheroid is shown. The material selected already has the values proposed on Table 4.

Once the prolate spheroid is modeled, the next step is to set up the simulation. This is done by setting the excitation, the mesh of the model, the boundaries of the simulation, the desired measurements and the solution parameters.

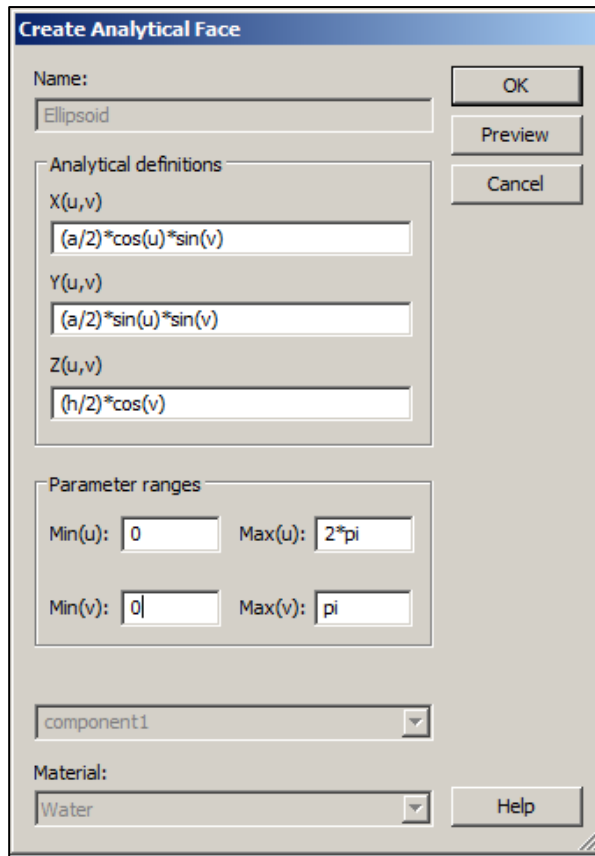


Figure 6. Prolate Spheroid Specifications.

The excitation of interest is a plane wave and can be defined with the information of figure 6. The different polarizations of interest are defined on table 5.

Table 5. Polarization Parameters for plane wave in CST.

Polarization	Propagation Vector	Field Vector
EHK	[1 0 0]	[0 0 86.83]
HEK	[1 0 0]	[0 86.83 0]
KEH	[0 0 1]	[0 -86.83 0]

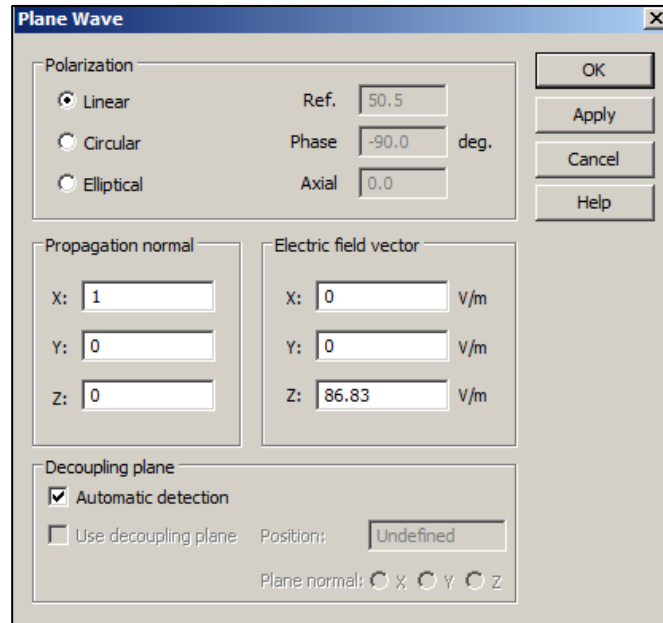


Figure 7. Plane wave specifications window in CST.

For the mesh, a good rule of thumb is to have at least 10 basis functions per wavelength as long as the computational resources can handle the model. If it is too much to handle, the mesh density can be reduced but it may cause a loss in accuracy in the simulation, it is an important trade off to have in mind. These properties can be seen on figure 8.

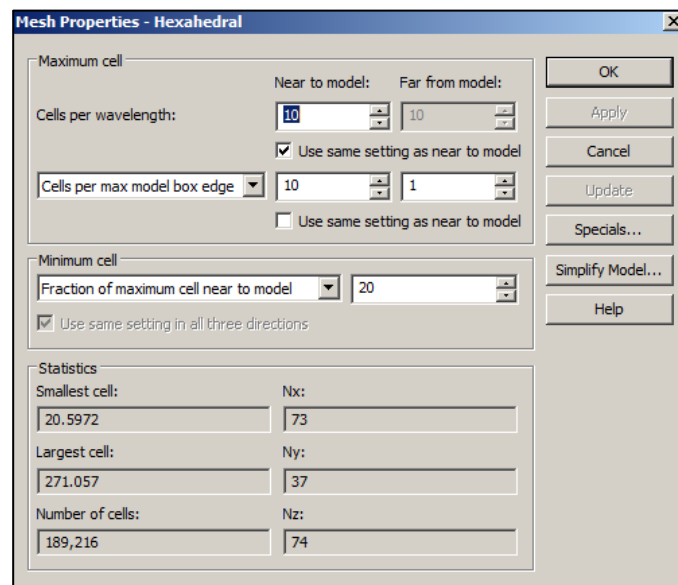


Figure 8. Mesh properties window in CST.

To extend the range of the simulations, the use of symmetry is very important. A lot of geometries have the advantage of also being electrically symmetrical. This symmetry allows reducing the numbers of unknowns needed to solve a problem using a numerical method. In case of CST electrical symmetry can be applied in all major planes of interest (XY, XZ, and YZ). Where to apply symmetry will depend on the source used. For a plane wave, symmetry depends on the direction of propagation and the direction of the electromagnetic fields. For the 3 polarizations used in this report, table 6 summarizes the different values needed for every scenario. If symmetry is applied in the wrong way, results may vary and become unusable.

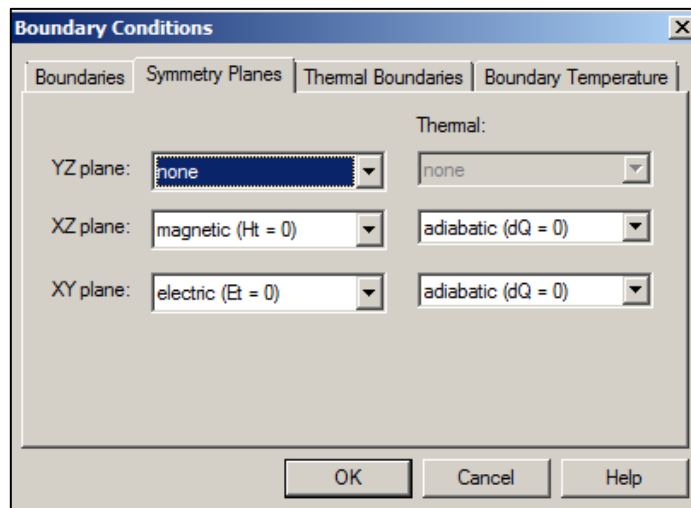


Figure 9. Symmetry planes window in CST.

Table 6. Symmetry parameters used in figure 8.

Polarization	YZ Plane	XZ Plane	XY Plane
EHK	None	Magnetic	Electric
HEK	None	Electric	Magnetic
KEH	Magnetic	Electric	None

The final step before running the simulation is to set the probes or “monitors” that will measure the quantity of interest, which in the case of whole-body SAR is the power loss in the body. The monitors are set in the frequencies of interest using the field monitor option of the simulation tab in CST. Once all these steps have been made, the simulation can be run. Once it is finished the results can be obtained from the navigation tree as follows: *1D Results >> Power >> Excitation >> Loss in Dielectric*. The results obtained here must be divided by the object’s mass which is obtained from the volume of the prolate spheroid and the density of the material, in this case water. For the dimensions of the prolate spheroid used, the mass is about 84.83 Kg.

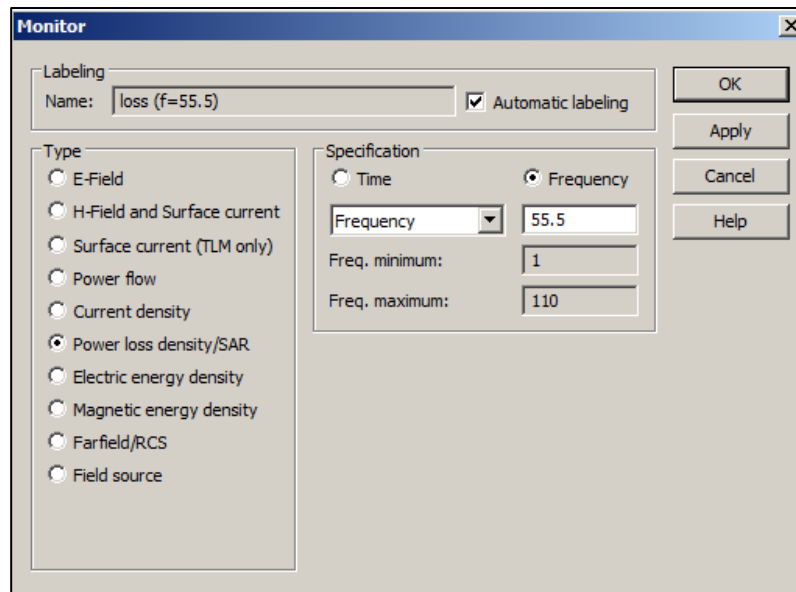


Figure 10. Monitor set up window in CST.

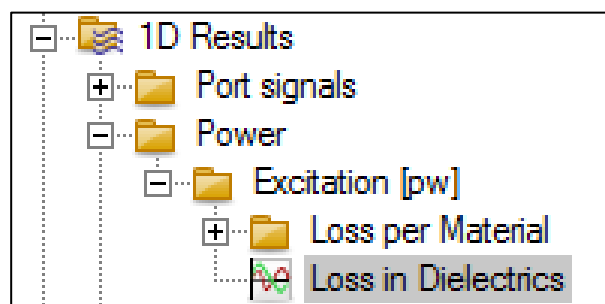


Figure 11. Results tab in CST.

4.1.2 Modeling of a prolate spheroid using CONCEPT-II

In CONCEPT-II the modeling of the prolate spheroid is done by using the CAD tools of the software. Once specified the dimensions of the spheroid, the next step is to set up the mesh density of the body. This can be done using the optimal mesh for a certain frequency or setting the values manually. When the optimal mesh tool is used, the geometry is discretized using the frequency of interest and a number of basis functions chosen by the user. The number of basis functions is between 8 and 12 for this type of bodies. All the model and mesh set up is done in the window of figure 12.

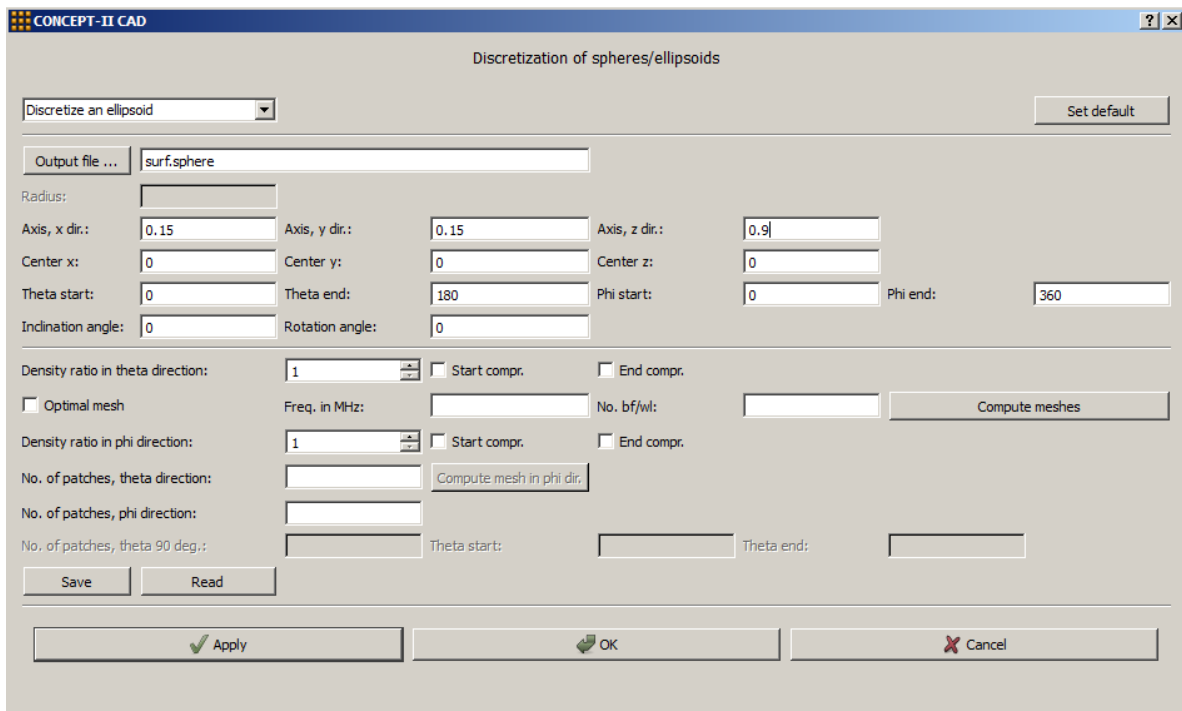


Figure 12. CAD tool for geometry modeling in CONCEPT-II.

Once defined the geometry with its mesh, it is necessary to set the source, the material properties and the frequency of interest. Like in CST, depending on the polarization used, there will be different values to set in the excitation and the symmetry. Even though, the prolate spheroid can use electrical symmetry to optimize calculations, CONCEPT-II doesn't have available all the possible combinations to fully make advantage of this tool.

CONCEPT-II only manages magnetic symmetry for the XZ and YZ plane, and electric symmetry for the XY plane. This means that in polarizations like HEK, the symmetry option is not available and thus the frequency range is heavily crippled for this scenario. For EHK the full symmetry can be used, which means that only a quarter of the geometry is needed for the simulation, but KEH can only manage half symmetry due to the “electrical symmetry” not being a real option in the general sense.

To set the excitation, there’s the option of using a plane wave which can be set in almost any direction. To use the polarizations of interest the window of figure 13 must be filled with the values of table 7. For a power density of $1\text{mW}/\text{cm}^2$, the electric field is set to a value of 86.83 V/m . Once this is set, the frequencies of interest can also be set up to start the simulation. The material values are also the same as used in the CST simulation.

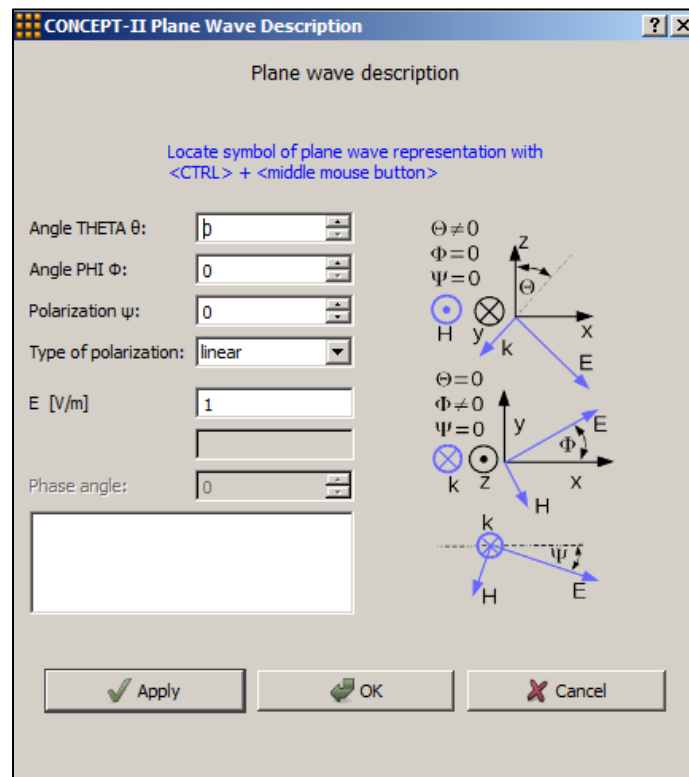


Figure 13. Plane wave description window in CONCEPT-II.

Table 7. Angle values for different polarizations on CONCEPT-II.

Polarization	θ	ϕ	ψ
EHK	90	180	180
HEK	270	0	270
KEH	180	180	0

Once the simulation is completed, it is necessary to calculate the power loss in the model. This can be done in the post-processing tab and using  to calculate the power flow through the structure. To calculate the power, another spheroid (slightly bigger) needs to be modeled. This new spheroid is used as the surface to calculate the power flow. The results obtained by this method represent the power absorbed by the spheroid.

4.2 Whole-body SAR on a prolate spheroid using full-wave simulators CST and CONCEPT-II

In this subchapter are the results of all the full-wave simulations performed using CST and CONCEPT-II for whole-body SAR measurements using different plane wave polarizations. For the CST simulations two computers were used: a local computer with 4 cores and 16 GB of RAM and a remote computer with 6 cores and 32 GB of RAM. For the CONCEPT-II simulations, a local computer with 4 cores and 16 GB was used initially but then for later simulations a server cluster was used which had 10 nodes available each one containing 6 CPUs and 32 GB of RAM.

4.2.1 EHK Polarization

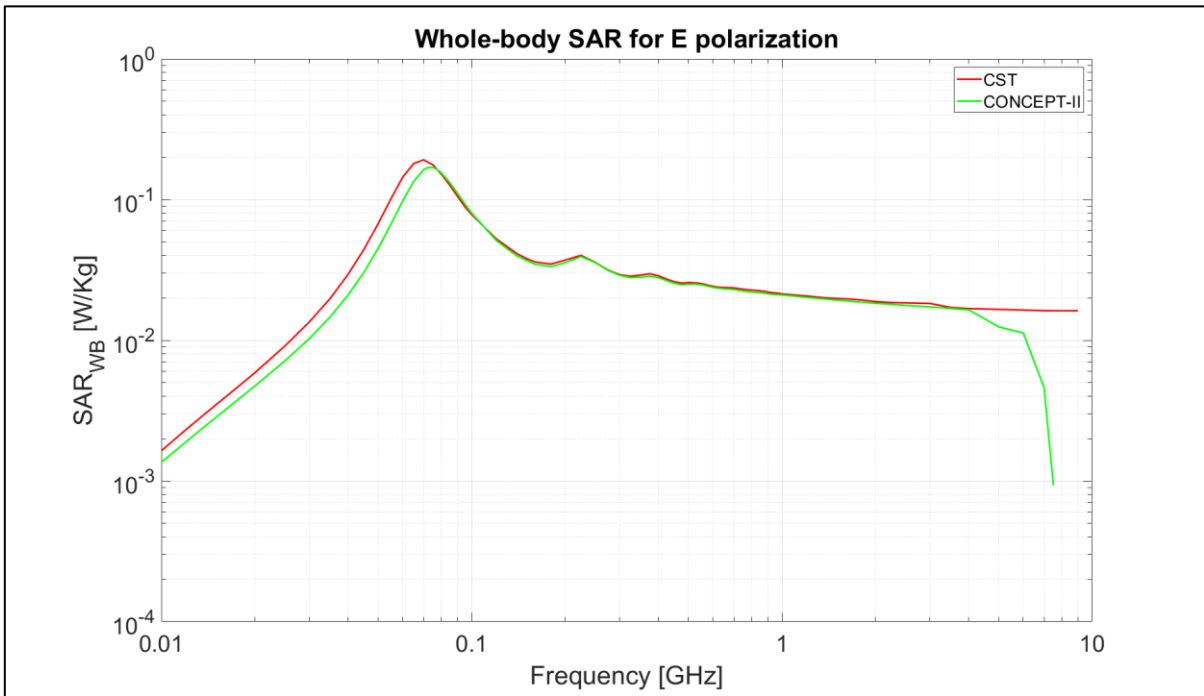


Figure 14. Whole-body SAR for E Polarization on CST and CONCEPT-II.

In figure 14, it can be seen that the obtained behavior for whole-body SAR with E polarization is similar to the one expected from figure SAR. Clearly, the exact values are different due to the differences in dimensions and material choices but the values follow the expected trend.

Both solvers have very similar results between them and also a similar reach in terms of computational power, which can be seen from the maximum frequency achieved in the simulations. Differences in values are found in the lower frequency range, from 10 MHz to the resonance frequency the values obtained in CONCEPT-II are a little bit lower than the ones obtained in CST. Once the resonance frequency is passed, the values from both solvers stay pretty close to each other up until 4 GHz where the solution obtained in CONCEPT-II starts to fall abruptly.

This fall is due to numerical limitations of the MoM implementation of CONCEPT-II where the damping of the body is so strong that the calculation of the internal fields starts to become very difficult to obtain and the values begin to lose accuracy. In tables 8 and 9 are summarized the computing power for each implementation and the parameters used in the simulations.

*

Table 8. CST model information for the calculation of whole-body SAR in E polarization.

Polarization	Computer	# CPUS	Mesh cells	Frequency	Time	bf/wl	Memory (MB)	Steps
EHK	Local	4	16848	10-100 (MHz)	00:00:08	10	120.97	23
EKH	Local	4	243600	100-500 (MHz)	00:01:10	10	793.39	19
EHK	Local	4	1987500	0.5-1 (GHz)	00:08:43	10	2756.3	22
EHK	Local	4	11215800	1-1.8 (GHz)	00:20:47	10	7410.81	5
EHK	Local	4	44331140	2-3 (GHz)	01:39:35	10	14368.13	5
EHK	Local	4	55492535	3-4 (GHz)	01:46:52	9	14089.52	2
EHK	Local	4	75721500	5 (GHz)	02:45:41	8	14877,1602	1
EHK	Remote	6	83755008	6 (GHz)	04:25:45	7	28139,9805	1
EHK	Remote	6	131483476	7 (GHz)	07:21:21	7	30639,3047	1
EHK	Remote	6	173837055	9(GHz)	15:53:14	6	30813,5078	1

* **bf/wl**: basis function per wavelength.

In table 8, we can see the different parameters used by CST to perform the simulations and also some results like the time it needed to finish a simulation, the number of frequency steps used in the simulation and the memory needed to run the simulation. It is clear that when going up in frequency the sweeps are harder to compute so the steps used in every simulation start to go down, also the number of basis functions per wavelength starts to go down due to the number of mesh cells being too big to handle, which is a tradeoff in terms of accuracy. To compute the 6 GHz simulation a more powerful computer was needed.

In the end, this kind of simulation is still very resource consuming, even with newer tools and much more processing power. For example, if the simulations were to be run using 10 basis functions from 8 GHz onwards it would be needed a much more powerful computer because CST requires 35 GB of memory only to solve the core model without including the memory needed to compute the monitors which calculate the measurements of interest. More information about the computing limitations can be read on subsection 4.3.

For CONCEPT-II, memory use works a little bit different whereas in CST the mesh density scales with the frequency dependently in CONCEPT-II the density is generated by the user and even if its formulation must take into account the frequency of interest, it is in no way bound by it. For this reason, in CONCEPT-II a unique mesh can work for a large frequency sweep. In table CO, the computing power used by CONCEPT-II is presented.

Table 9. CONCEPT-II model information for the calculation of whole-body SAR in E polarization.

Polarization	Computer	# CPUS	Unknowns	Frequency	Time (HH:MM:SS)	bf/wl	Memory (GB)	Steps
EHK	Local	4	1748	10-100 (MHz)	00:05:00	8	0,046	23
EHK	Cluster	24	6018	100-500 (MHz)	00:05:49	8	0,54	18
EHK	Cluster	60	136022	1-7 (GHz)	34:48:31	8	275,70	10

Another simulation run in CST consisted in varying the mesh density of the spheroid to see the changes in the values obtained. These results are shown in figure 15.

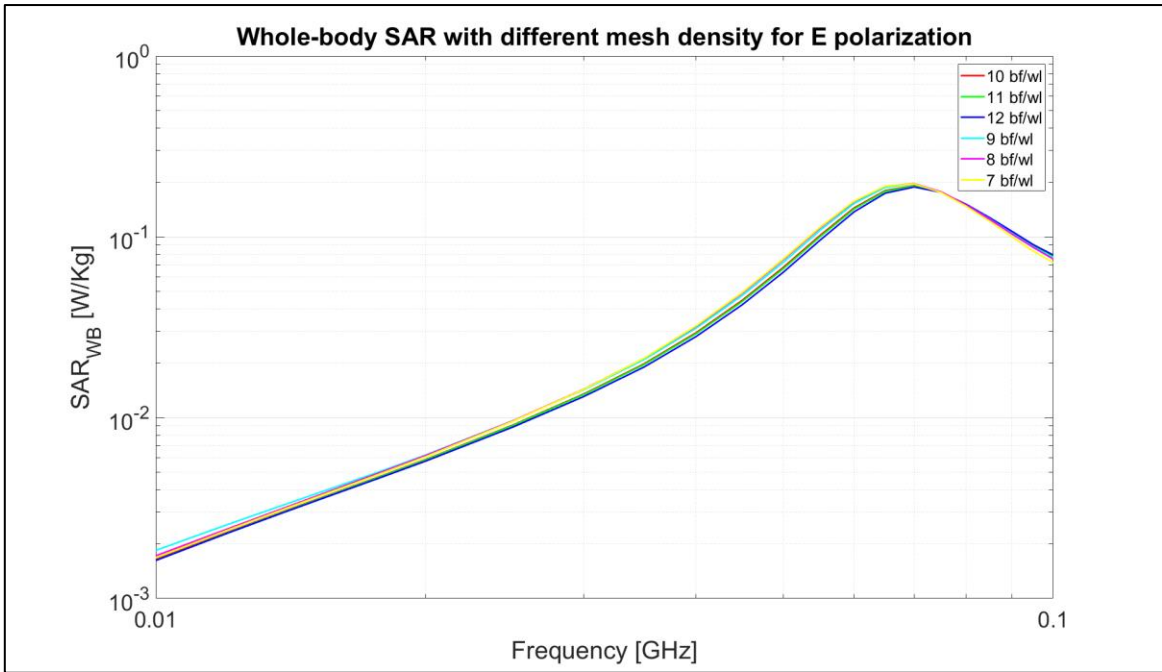


Figure 15. Whole-body SAR with different mesh density for E Polarization from 10 MHz to 100 MHz.

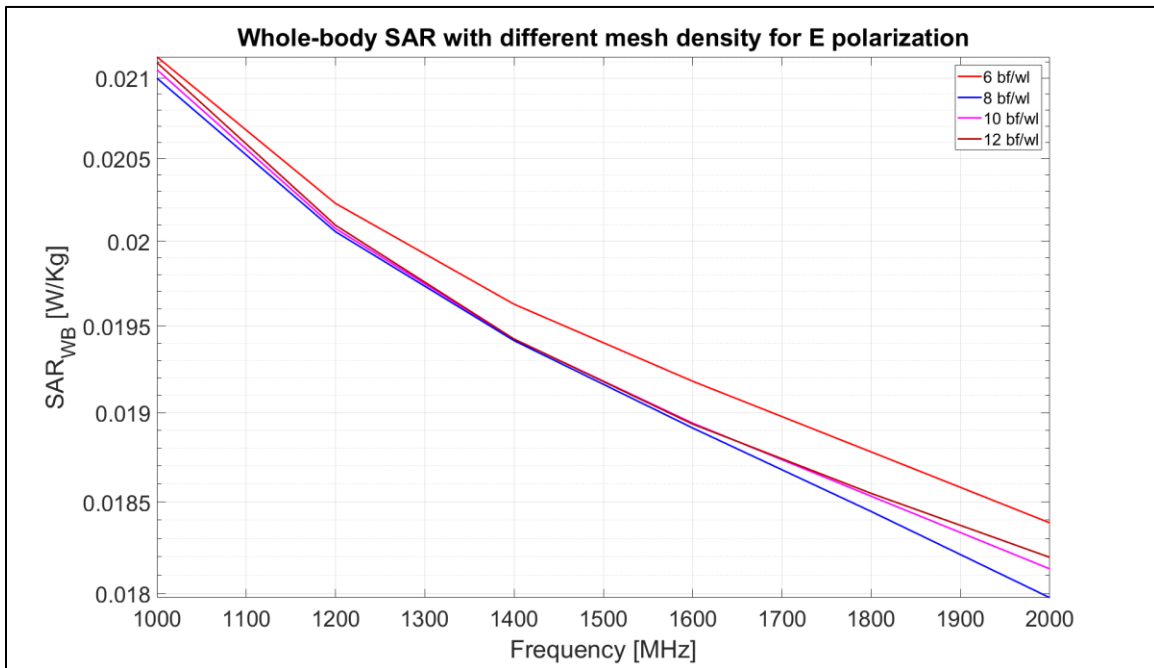


Figure 16. Whole-body SAR with different mesh density for E Polarization from 1 GHz to 2 GHz.

In figure 15, the effect of varying the mesh density in CST for the low frequency end of the whole-body SAR in E polarization can be seen. Even though, the behavior

and values are quite similar, this trend starts to change when we reach the high frequency end due to the fast-changing fields which need a very dense mesh, meaning that this kind of variations increase. This also means that there is a trade-off of accuracy vs memory the higher we go in frequency. The change can be seen in figure 16.

4.2.2 HEK Polarization

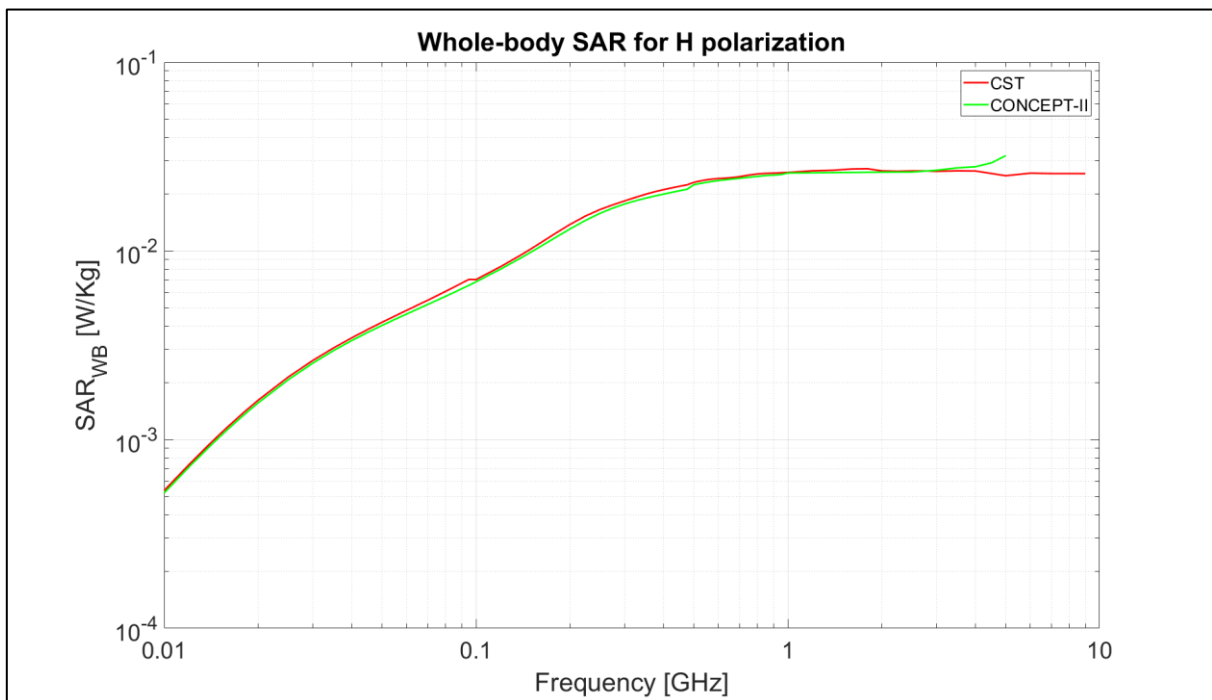


Figure 17. Whole-body SAR for H Polarization on CST and CONCEPT-II.

In figure 17, we see that for H polarization, the results between both solutions are quite similar not only to the theory but also between them; also as with E polarization CST has more range in terms of frequency than CONCEPT-II. The details of each simulation can be seen in tables 10 and 11.

Table 10. CST model information for the calculation of whole-body SAR in H polarization.

Polarization	Computer	# CPUS	Mesh cells	Frequency	Time	bf/wl	Memory (MB)	Steps
HEK	Local	4	16848	10-100 (MHz)	00:00:08	10	121.1	23
HEK	Local	4	239540	100-500 (MHz)	00:00:57	10	762.44	19
HEK	Local	4	1987500	0.5-1 (GHz)	00:08:21	10	2750.3	22
HEK	Local	4	11215800	1-1.8 (GHz)	00:19:49	10	6900.43	5
HEK	Local	4	44331140	2-3 (GHz)	01:33:37	10	14526.70	5
HEK	Local	4	55492535	3-4 (GHz)	01:36:22	9	15140,2266	2
HEK	Local	4	75721500	5 (GHz)	02:56:05	8	15130,1016	1
HEK	Remote	6	83755008	6 (GHz)	07:57:43	7	22122,2852	1
HEK	Remote	6	131483476	7 (GHz)	07:25:15	7	30888,9727	1
HEK	Remote	6	173837055	9(GHz)	11:45:03	6	30966,9648	1

Table 11. CONCEPT-II model information for the calculation of whole-body SAR in H polarization.

Polarization	Computer	# CPUS	Unknowns	Frequency	Time (HH:MM:SS)	bf/wl	Memory (GB)	Steps
HEK	Cluster	24	8592	10-100 (MHz)	00:20:50	8	1,1	25
HEK	Cluster	24	8592	100-1000 (MHz)	00:21:53	8	1,1	38
HEK	Cluster	60	121656	1-5 (GHz)	17:52:25	8	220,54	10

CST allows for more simulations than CONCEPT-II but starts to sacrifice accuracy from 5 GHz; on the other side, CONCEPT-II suffers from the lack of a symmetry option for the HEK polarization which makes the simulation scale heavily in comparison to EHK and KEH polarizations. However, it is still faster (per frequency point) than a simulation performed in CST.

4.2.3 KEH Polarization

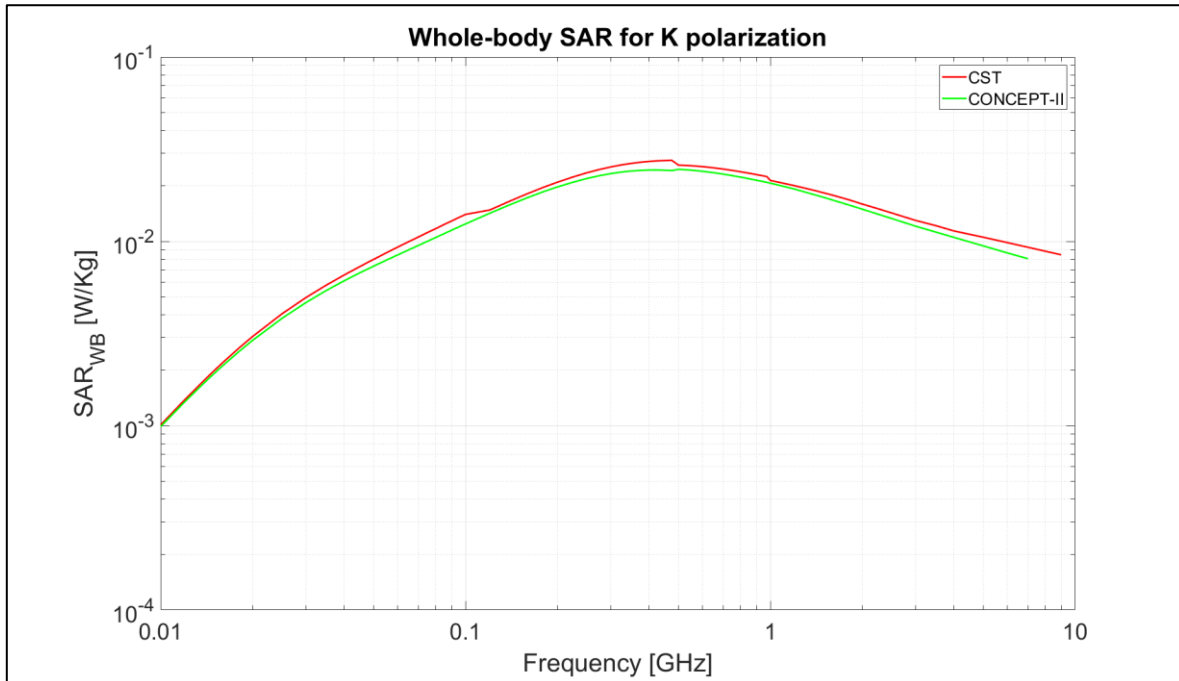


Figure 18. Whole-body SAR for H Polarization on CST and CONCEPT-II.

As with previous polarizations, the results obtained for K polarization match the behavior expected from theory and between themselves. One important detail to take into account with this scenario is that the values from 1 GHz up to 22 GHz were originally estimated values [1]. For that reason, the results obtained from these simulations are important because they describe a behavior that was unable to be measured with analytical tools.

Another important observation is that for K polarization, CONCEPT-II can reach a maximum of 7 GHz which is equal to the limit obtained by the E polarization, although in this scenario the values for the Whole-body SAR can be calculated and still match the results from CST.

Table 12. CST model information for the calculation of whole-body SAR in K polarization.

Polarization	Computer	# CPUS	Mesh cells	Frequency	Time	bf/wl	Memory (MB)	Steps
KEH	Local	4	16055	10-100 (MHz)	00:00:09	10	121.2	23
KEH	Local	4	242760	100-500 (MHz)	00:01:03	10	783.24	19
KEH	Local	4	2000061	0.5-1 (GHz)	00:08:55	10	2799.08	22
KEH	Local	4	11265648	1-1.8 (GHz)	00:22:45	10	7751.63	5
KEH	Local	4	32245056	2-3 (GHz)	01:05:23	10	13832.59	5
KEH	Local	4	55648852	3-4 (GHz)	02:04:49	9	14573,707	2
KEH	Local	4	53895072	5 (GHz)	03:16:44	7	14945,8633	1
KEH	Remote	6	83755008	6 (GHz)	07:55:20	7	24757,1367	1
KEH	Remote	6	131433747	7(GHz)	07:21:21	7	28139,9805	1
KEH	Remote	6	174192550	9(GHz)	12:31:27	6	30937,1719	1

Table 13. CONCEPT-II model information for the calculation of whole-body SAR in K polarization.

Polarization	Computer	# CPUS	Unknowns	Frequency	Time (HH:MM:SS)	bf/wl	Memory (GB)	Steps
KEH	Cluster	24	8592	10-100 (MHz)	00:13:45	8	1,1	25
KEH	Cluster	24	8592	100-1000 (MHz)	00:21:53	8	1,1	38
KEH	Cluster	60	136022	1-7 (GHz)	38:35:58	8	275,70	10

Results from tables 12 and 13 keep the trend of previous simulations, with an potential increase of number of mesh cells or unknowns, that reflects in memory use. CONCEPT-II is still the faster approach but the memory demand gets higher for frequencies that exceed 5 GHz.

4.2.4 Whole-body SAR, final comparisons and other simulations

In this section are presented other simulations that were performed using the EHK polarization with the purpose of giving more insight in terms of the resonance frequency. Also there are results of the 3 main polarizations against each other for each numerical solver.

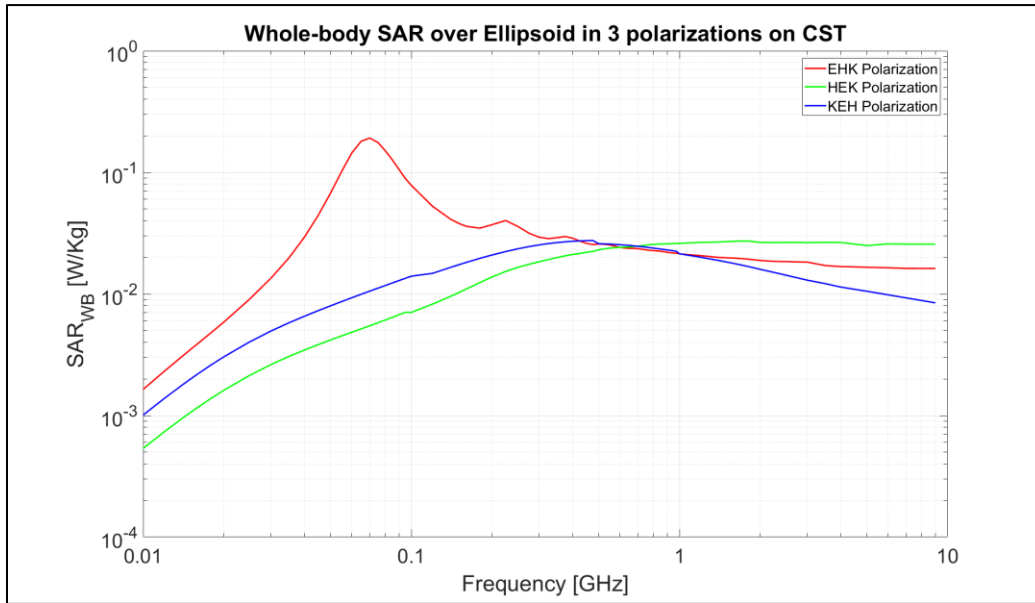


Figure 19. Whole-body SAR for 3 Polarizations in CST.

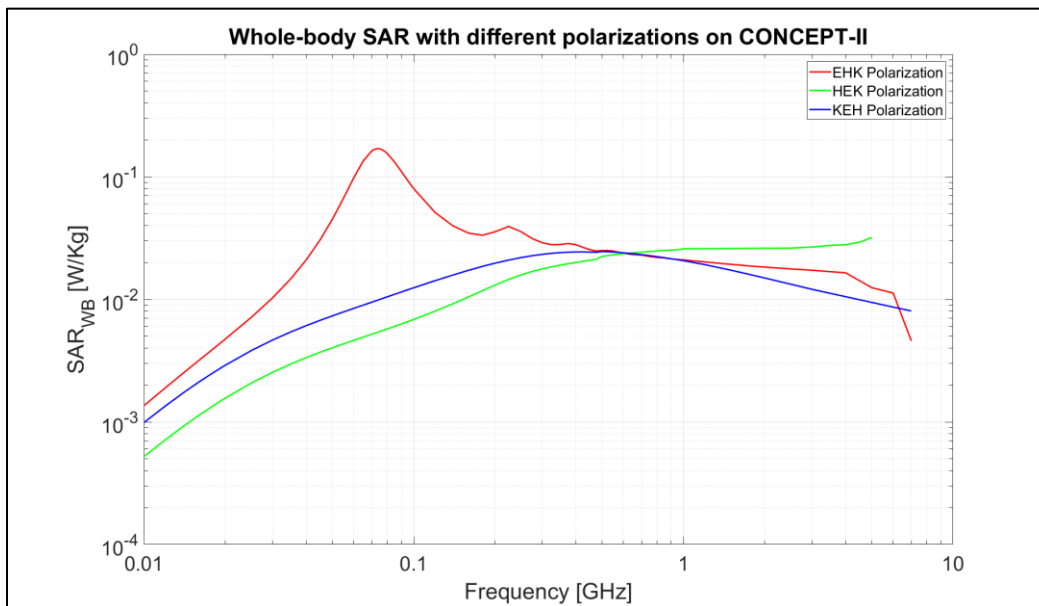


Figure 20. Whole-body SAR for 3 Polarizations in CONCEPT-II.

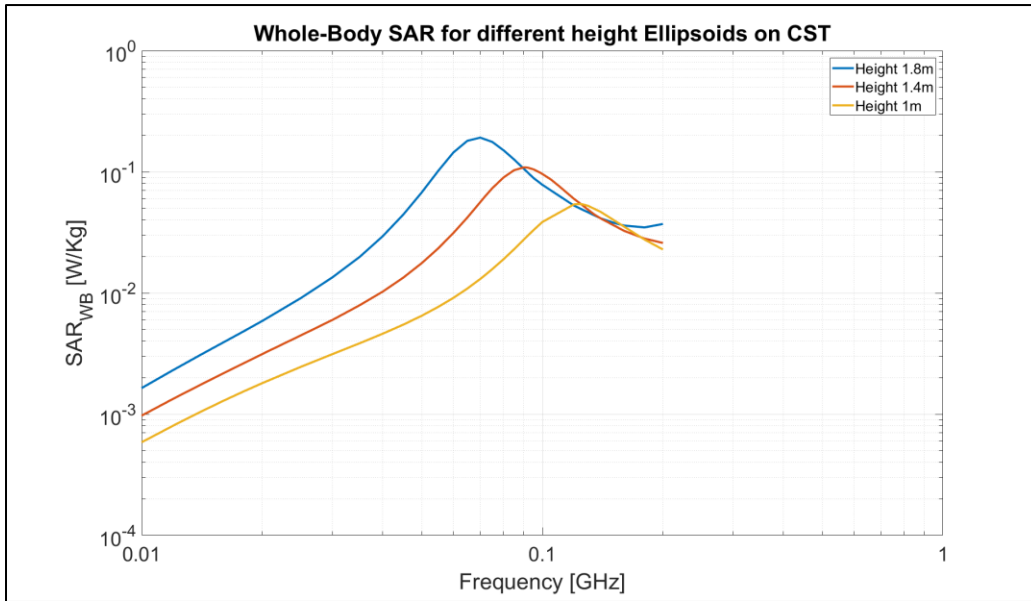


Figure 21. Whole-body SAR for 3 different size prolate spheroids in CST.

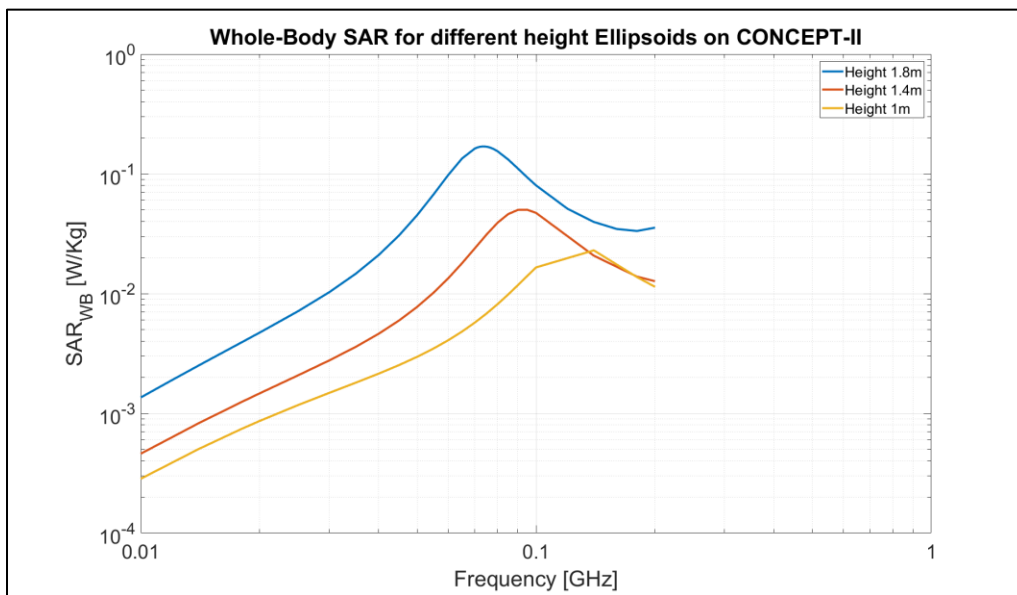


Figure 22. Whole-body SAR for 3 different size prolate spheroids in CONCEPT-II.

The effect of varying the height is described on [21]. If the ratio between the axes goes down, the resonance frequency shifts to a higher value. This is important because it marks a difference between the analyses done for smaller models (like children) versus the ones done in bigger models (adults). For the CONCEPT-II

results, the exact value of the resonance frequency is a bit rough to find due to the frequency sweep chosen.

4.3 Computational limitations on full-wave simulations

From the previous subsections, it can be seen that there is still a limit in terms of how far these numerical methods can go to really obtain accurate results. For some models the limit is higher than for others and it also depends on the type of problem that is being worked.

In the problem of interest, the number of elements to solve starts to increase drastically as frequency goes up. For example, using the recommended amount of basis functions for the prolate spheroid described in section 3.1 on CST gives a warning that the number of cells needed to compute the problem exceeds 1 billion cells. This message is shown around 20 GHz and basically tells that from that frequency and up, the processing power needed for those computations is enormous. In table 14, the number of mesh cells is showed with a column of status which tells if the program pops up the warning or not.

Table 14. Mesh cells in CST using 10 basis functions per wavelength.

Frequency (GHz)	Mesh Cells	Status
10	1,168,676,136	No warning
15	3,927,110,544	
20	9,286,622,016	Warning
30	31,354,101,216	
40	74,292,276,128	
50	145,070,824,800	
60	250,738,794,432	
70	398,020,714,689	
80	594,240,318,756	
90	846,006,700,000	
100	1,160,404,930,140	

In relation to the previous table if the simulation does not show a warning, the amount of RAM needed to compute the simulations is pretty heavy. This can be seen in table 15.

Table 15. Memory needed to perform prolate spheroid simulations using a model with 10 basis functions per wavelength.

Frequency (GHz)	Memory (GB)
6	15
7	24
8	35
9	50
10	88

Based on these tables and the results from past subsections, the frequency limit reached in this report regarding the use of CST for simulations of Whole-body SAR measurements is 9 GHz for a prolate spheroid modeled using 6 basis functions per wavelength. With a computer with 128 GB of RAM a simulation using 10 basis functions per wavelength could be done but higher than that it becomes potentially harder to have the resources necessary to run these kinds of simulations.

In terms of CONCEPT-II, the frequency limit reached is a little bit different; because, the limit reached to actually run a simulation is not the same limit reached to actually calculate the EM fields in a correct way. For example, with all the power available in the cluster used for CONCEPT-II simulations (320 GB RAM, 60 CPUs) the limit for E polarization simulations is 7 GHz but the fields obtained for values higher than 4 GHz start to behave in a way that is not compatible to other solutions available like CST or [1].

There are also the symmetry options which are limited in CONCEPT-II. This makes that the H polarization gets a lower limit (5 GHz) while the others can reach a higher one. Table 16 gives an idea of the memory required to run these type of simulations, even if they are faster than a CST simulation, the memory capability makes them harder to run when trying for higher frequencies.

Table 16. Memory required for running simulations in CONCEPT-II for a prolate spheroid with optimized mesh for E and K polarizations.

Frequency (GHz)	Unknowns	Memory (GB)
5	59930	53.52
6	86788	112.24
7	118990	210.98
7.5	136022	275.70
7.8	147434	323.90
8	154350	355.00
9	196380	574.66
10	241590	869.72

5. Influence of material selection on EM radiation problems

In this section the electrical properties of water are studied using a 1D model of a reflection problem. The reason of this approach is that when reaching the high frequency region (10 GHz - 100 GHz+), the size of the wavelength is decreasing to a millimeter size. When this happens, the size of the wave is pretty small in comparison to the dimension of the body of interaction. This opens the possibility of using the one dimensional approach to study the effects of the incident wave at an interface level and obtain different helpful relations that can help in the understanding of the interactions between electromagnetic radiation and our bodies.

One important point is that materials can be modeled as frequency independent or frequency dependent. Most of the biological tissues have a frequency dependent behavior and even though water is not a tissue it also exhibits this behavior. To model a frequency dependent material there are different approaches, some are simple and others are very complex and in some cases there is the need of using experimental results to obtain a fitting curve to describe the behavior of a material.

In this section, the effects of an incident plane wave over a “wall” of water will be studied, comparing the differences if water is defined as a frequency dependent material or frequency independent and also if the angle of incidence of the wave is perpendicular to the surface or different.

5.2 Perpendicular incidence of a plane wave on a water surface

In this scenario, the wave propagates in a perpendicular direction to the surface of interest. The power density of the wave is 1 mW/cm^2 and the two interfaces are air and water. First the frequency independent scenario will be studied and then the frequency dependent. The values of interest are the reflection and transmission coefficient, the surface impedance, the attenuation and phase constant and the skin

effect of the material. All the values were obtained by coding the following set of equations in MATLAB. The problem of interest is shown in figure 23.

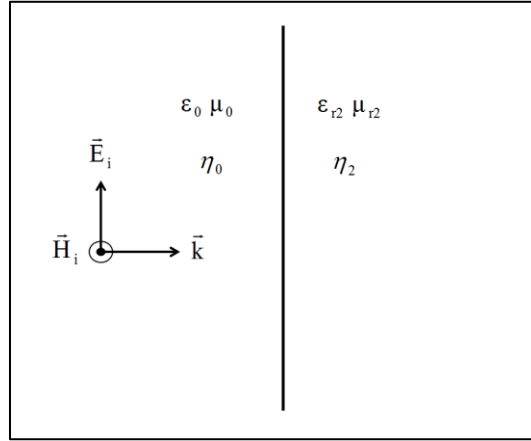


Figure 23. 1D Perpendicular incidence model.

5.2.1 Frequency Independent Material (FIM) Model of Water

For the frequency independent material (FIM) model definition of Water, the values from CST were used. Here a constant value for the real term of the complex permittivity is used and the imaginary part is obtained from the conductivity value given by the material definition.

$$\epsilon'_{r2} = 78 \quad (19)$$

$$\sigma = 1.59 \text{ [S/m]} \quad (20)$$

$$\epsilon = \epsilon'_{r2} - j\epsilon''_{r2} = \epsilon'_{r2} - j \sigma / \omega \epsilon_0 \quad (21)$$

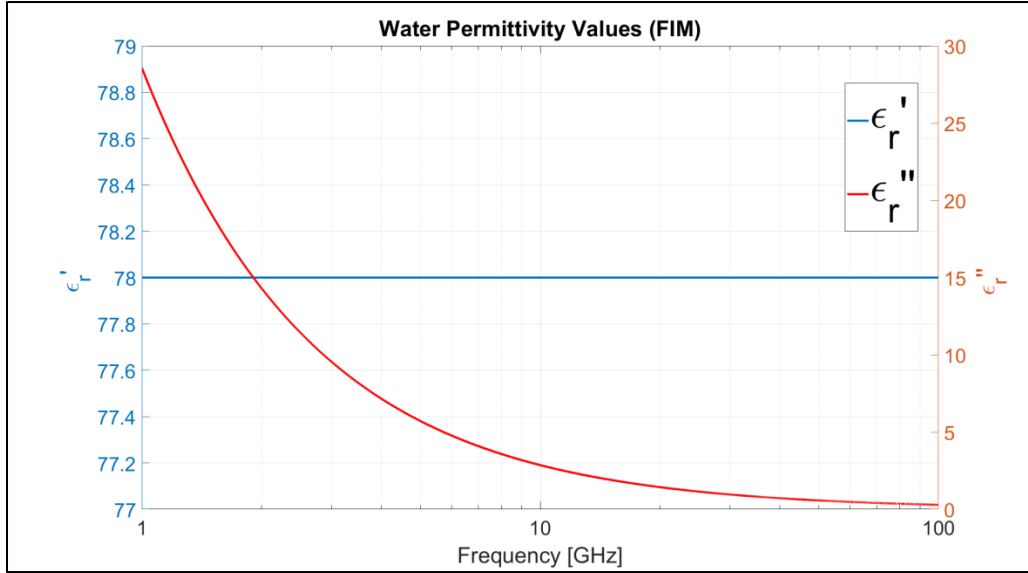


Figure 24. Water electric permittivity values for a FIM model.

Once the permittivity is defined the next step is to calculate the wave impedance of the material, which is obtained with the following equation. It is important to note that this values change in frequency and that the propagation constant needs to be calculated first. From the propagation constant the attenuation and phase constant are calculated.

$$\gamma = \alpha + j\beta = j\omega\sqrt{\mu\epsilon} = j\omega\sqrt{\mu\epsilon'(1 - j\sigma/\omega\epsilon_0)} \quad (22)$$

$$\eta_2 = j\omega\mu/\gamma \quad (23)$$

$$\eta_2 = j\omega\mu/\gamma = \frac{j\omega\mu}{\omega\sqrt{\mu\epsilon}} = \sqrt{\frac{\mu_{r2}\mu_0}{\epsilon_0(\epsilon_{r2} - j\epsilon_{r2})}} \quad (24)$$

$$\alpha = Re(\gamma) \quad (25)$$

$$\beta = Im(\gamma) \quad (26)$$

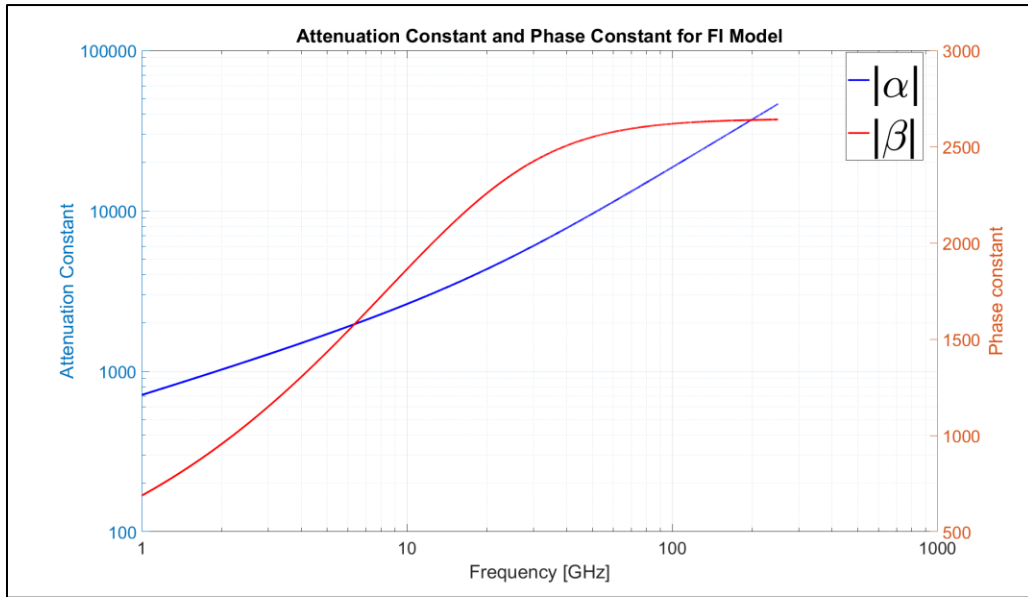


Figure 25. Attenuation and phase constant values for a FIM model.

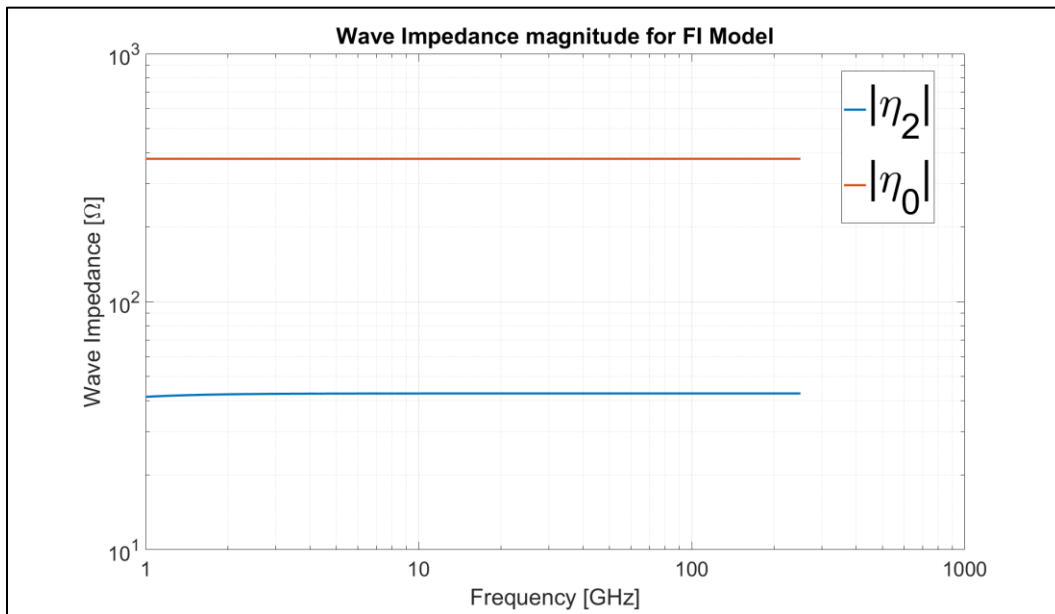


Figure 26. Wave impedance values for a FIM model.

Due to the behavior of the complex permittivity, the phase constant starts to saturate at a 100 GHz to a value of 2600 approximately. This behavior is also seen on the wave impedance described on figure 26. Once the wave impedance has been calculated, the next step is to obtain the reflection and transmission coefficients, which are obtained with the following relations.

$$\eta_0 = \sqrt{\mu_0/\epsilon_0} = 120\pi \approx 377\Omega \quad (27)$$

$$\Gamma = \frac{\eta_2 - \eta_0}{\eta_2 + \eta_0} = |\Gamma|e^{j\theta_\Gamma} \quad (28)$$

$$\tau = 1 + \Gamma = |\tau|e^{j\theta_\tau} \quad (29)$$

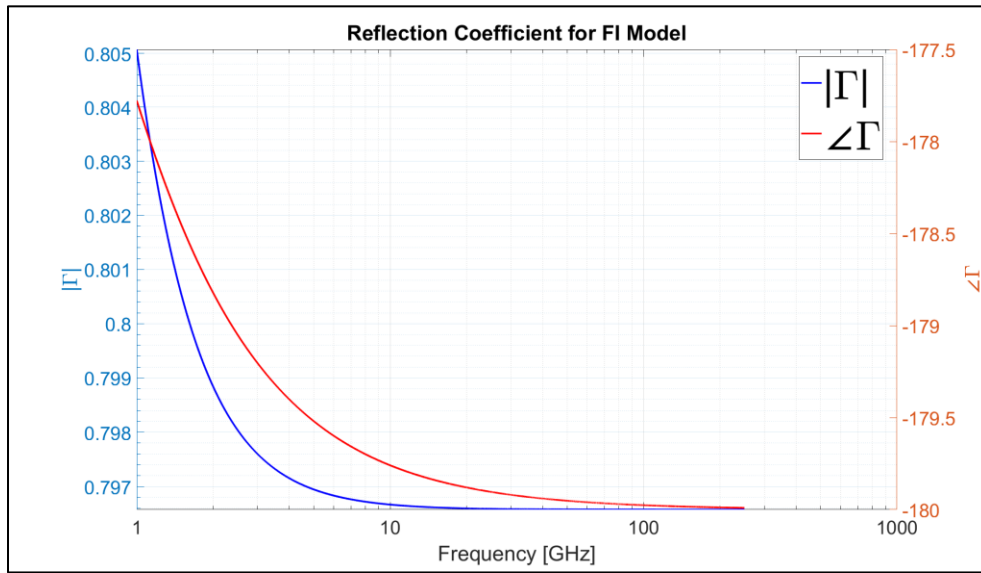


Figure 27. Reflection coefficient values for a FIM model.

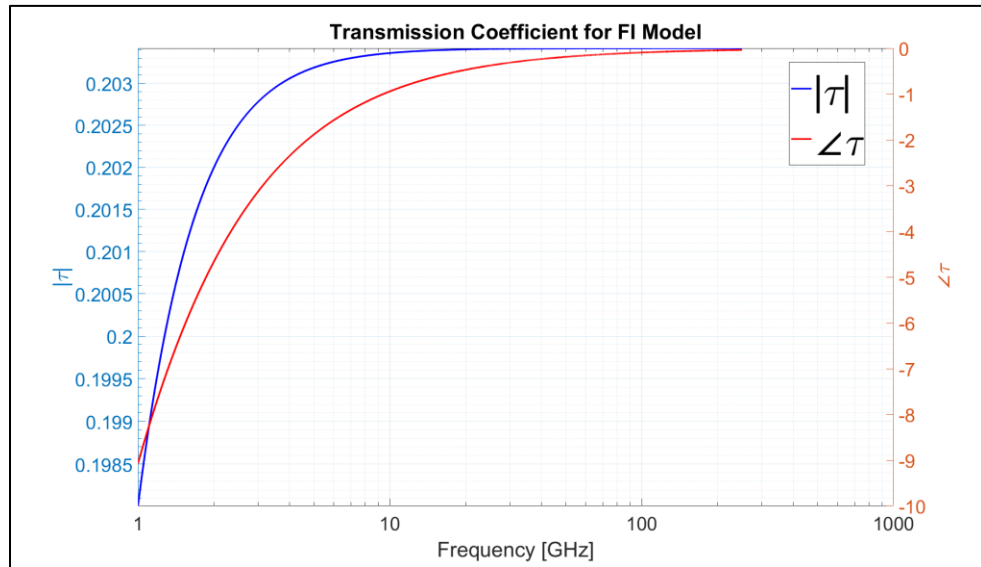


Figure 28. Transmission coefficient values for a FIM model.

5.2.2 Frequency Dependent Material (FDM) Model of Water

Unfortunately water does not behave as a frequency independent material; this means that to understand the effects of radiation on water a different approach is needed. Water as a frequency dependent material can be modeled using different methods, the simplest one is using a Debye relaxation model which gives a good approach but starts to lose accuracy when reaching higher frequencies.

That is why in this report the method used is the one described by Liebe in [23], which is a method based on the Debye approximation but using a fitting curve based on experimental results to increase the accuracy of the values. This method takes into the account the effects of temperature and for the calculation a temperature of 25°C was chosen. The next sets of equations are the ones used to obtain the real and imaginary part of the complex permittivity of water as a function of frequency. With the permittivity the attenuation and phase constant can be obtained using eq. (22).

$$\varepsilon_0 = 77.66 - 103.3\theta \quad (30)$$

$$\varepsilon_1 = 0.0671\varepsilon_0 \quad (31)$$

$$\gamma_1 = 20.20 + 146.4\theta + 316\theta^2 \text{ GHz} \quad (32)$$

$$\varepsilon_2 = 3.52 + 7.52\theta \quad (33)$$

$$\gamma_2 = 39.8\gamma_1 \quad (34)$$

$$\theta = 1 - \frac{300}{273.15 + T(^{\circ}C)} \quad (35)$$

$$\varepsilon'_{r2} = \frac{\varepsilon_0 - \varepsilon_1}{1 + \left(\frac{f}{\gamma_1}\right)^2} + \frac{\varepsilon_1 - \varepsilon_2}{1 + \left(\frac{f}{\gamma_2}\right)^2} + \varepsilon_2 \quad (36)$$

$$\epsilon_{r2}'' = \frac{\epsilon_0 - \epsilon_1 \left(\frac{f}{\gamma_1}\right)}{1 + \left(\frac{f}{\gamma_1}\right)^2} + \frac{\epsilon_1 - \epsilon_2 \left(\frac{f}{\gamma_2}\right)}{1 + \left(\frac{f}{\gamma_2}\right)^2} \quad (37)$$

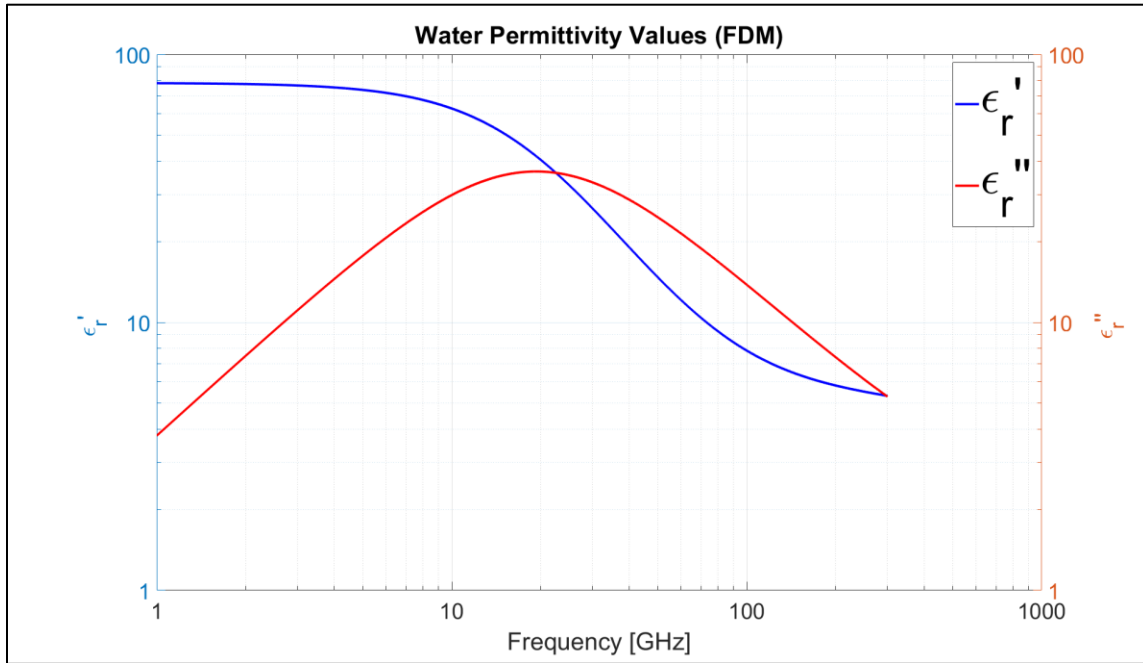


Figure 29. Water electric permittivity values for a FDM model.

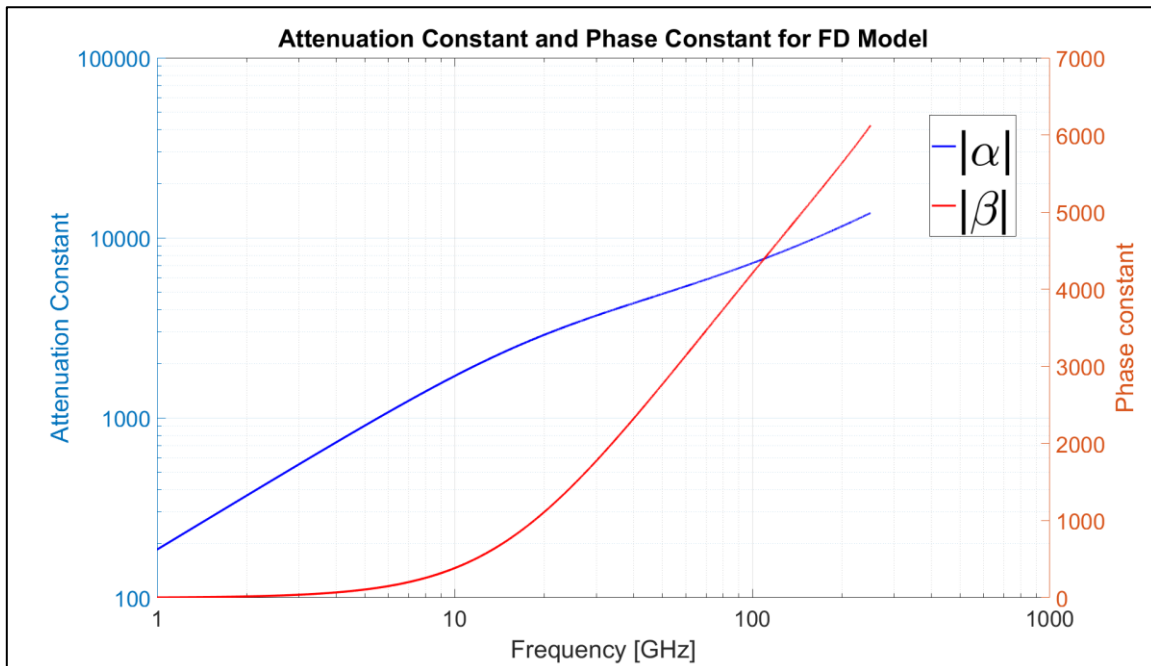


Figure 30. Attenuation and phase constant values for a FDM model.

Once the permittivity is obtained, the next step is to obtain the wave impedance of water. Using eq. (24) the wave impedance behaves as:

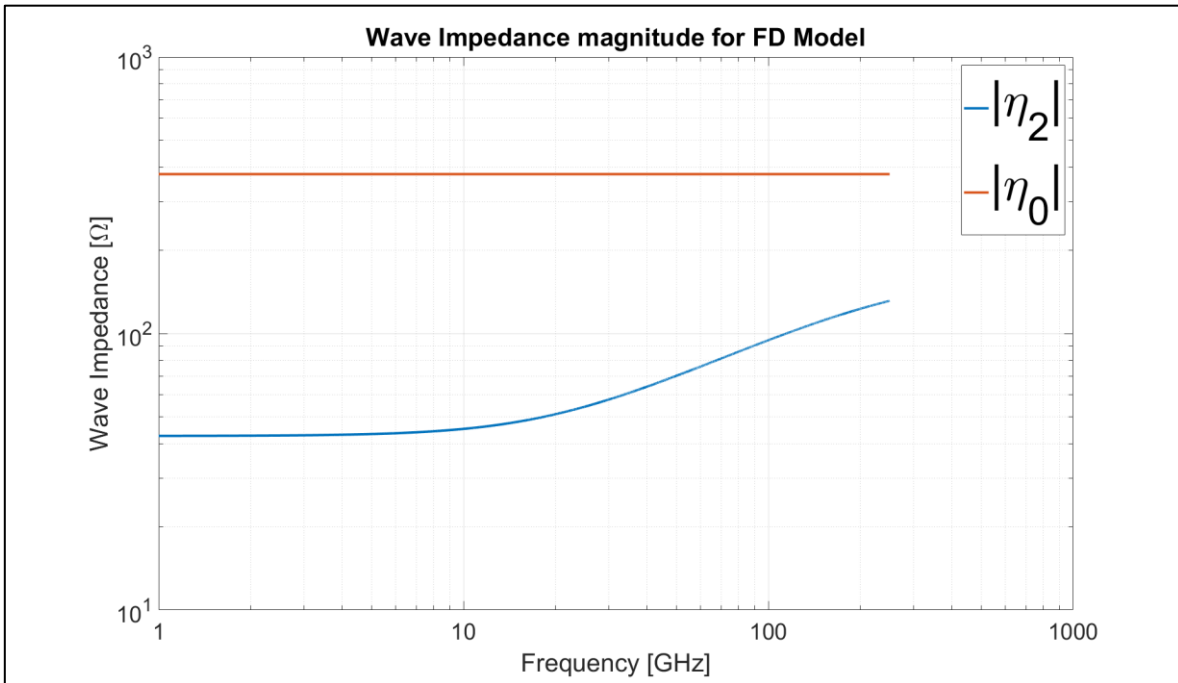


Figure 31. Wave impedance values for a FDM model.

From figures 29 and 30, the differences between models start to show. Apart from the obvious changes between the real and imaginary parts of the electric permittivity; the phase constant in the FDM model does not saturates and the wave impedance shows a very different behavior, it starts going up instead of converging to a single value. Finally, using equations (28) and (29) the transmission and reflection coefficients are calculated.

In regard to the material properties of the model, a visible difference is seen between the frequency dependent model and the frequency independent one. Attenuation constants for both model have a similar behavior, while the phase constant for both models varies heavily with one saturating (FIM) and the other with a steady grow (FDM).

Another important difference is the wave impedance behavior between both models. While for the frequency independent the real part of the complex permittivity is constant, the other model's real part start decreasing in frequency while the imaginary part starts increasing.

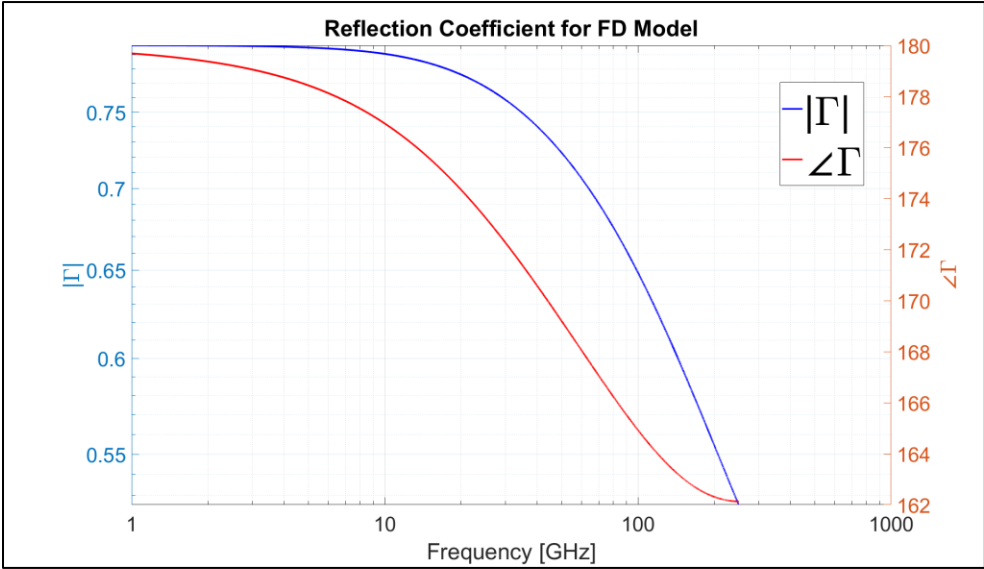


Figure 32. Reflection coefficient values for a FDM model.

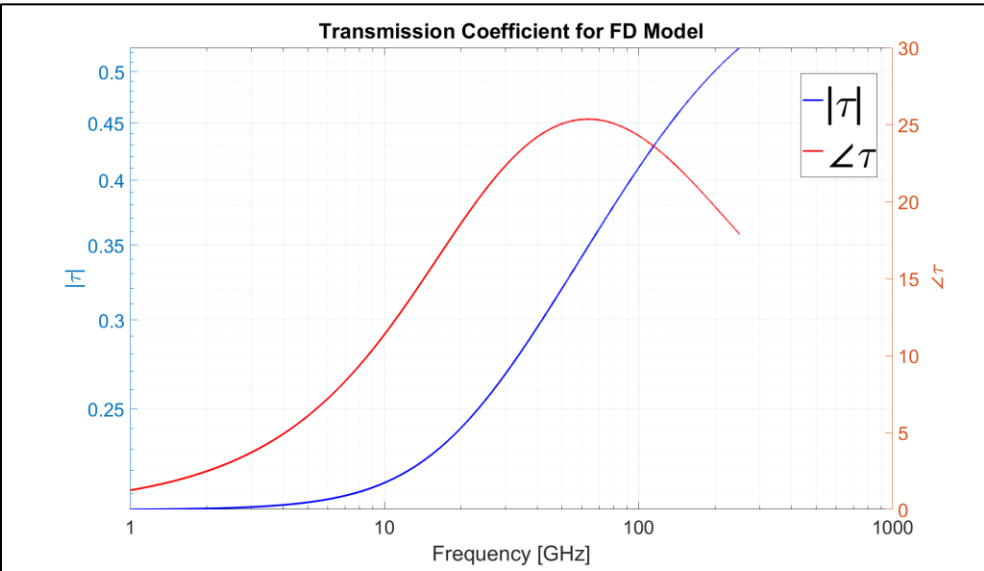


Figure 33. Transmission coefficient values for a FDM model.

5.3 General incidence of a plane wave on a water surface

While the 1D perpendicular incidence approach gives very valuable information, it is far from real scenarios. In limited cases, the plane wave will travel perpendicular to a surface, normally the direction of the propagation vector has an angle of incidence with respect to the surface plane and these changes the way reflections, transmissions and power behave in the material. The problem of interest is in figure 30.

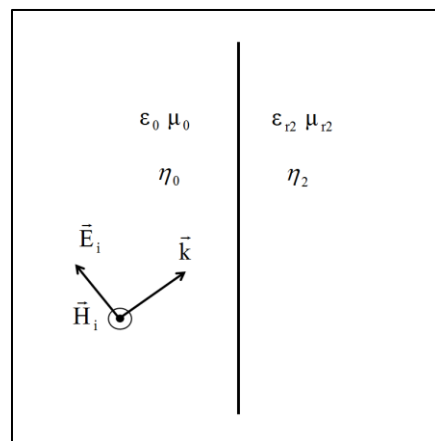


Figure 34. 1D General incidence model.

The same material definitions from previous subsections were used for the FIM model and the FDM model, the differences are in the definition of the reflection and transmission coefficients. A wave with a general direction can be divided in two major components, one that travels parallel to the plane of interest and one that travels perpendicular to it; this components can be obtained from the incidence angle of the wave regarding the plane of incidence and from the transmission angle of the wave.

These angles shape the form of the reflection and reflection coefficients where there is a reflection coefficient for the perpendicular component and one for the parallel. This also applies to the transmission coefficient and the following set of equations help understand this behavior.

$$\Gamma_{\perp} = \frac{\eta_2 \cos \theta_i - \eta_0 \cos \theta_t}{\eta_2 \cos \theta_i + \eta_0 \cos \theta_t} \quad (38)$$

$$\Gamma_{\parallel} = \frac{\eta_2 \cos \theta_t - \eta_0 \cos \theta_i}{\eta_2 \cos \theta_t + \eta_0 \cos \theta_i} \quad (39)$$

$$\tau_{\perp} = \frac{2\eta_2 \cos \theta_i}{\eta_2 \cos \theta_i + \eta_0 \cos \theta_t} \quad (40)$$

$$\tau_{\parallel} = \frac{2\eta_2 \cos \theta_i}{\eta_2 \cos \theta_t + \eta_0 \cos \theta_i} \quad (41)$$

In the report, the incidence angle was chosen with an increase of 15° up until 60° to showcase the behavior of the reflection and transmission coefficients. The angle of transmission for the calculations is obtained from the following equation.

$$\theta_t = \sin^{-1} \left(\sqrt{\frac{\mu_1 \epsilon_1}{\mu_2 \epsilon_2}} \sin \theta_i \right) \quad (42)$$

5.3.1 Frequency Independent Material (FIM) Model of Water

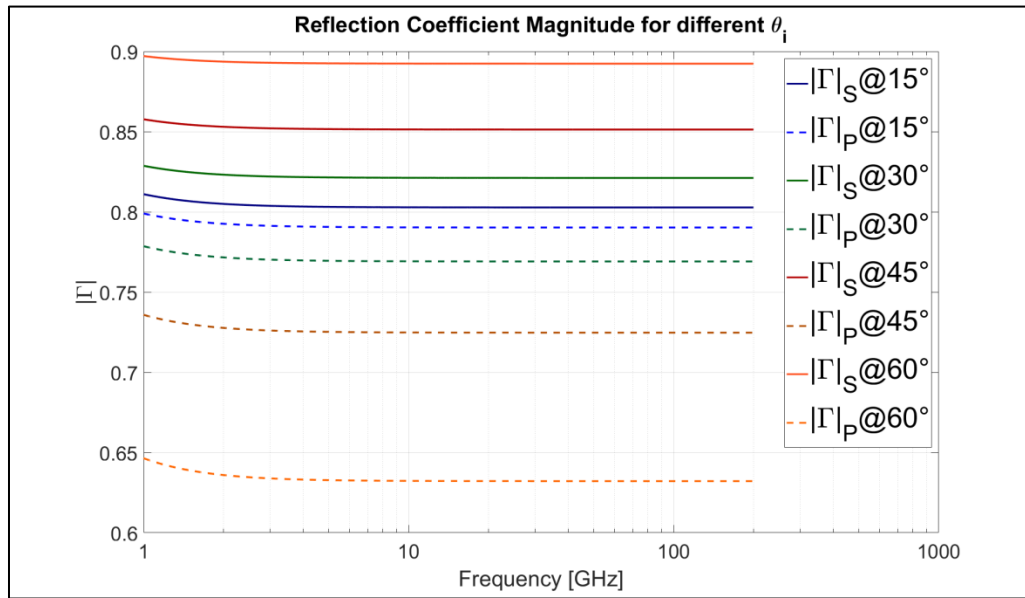


Figure 35. Reflection coefficient values for a FIM model with different angles on incidence.

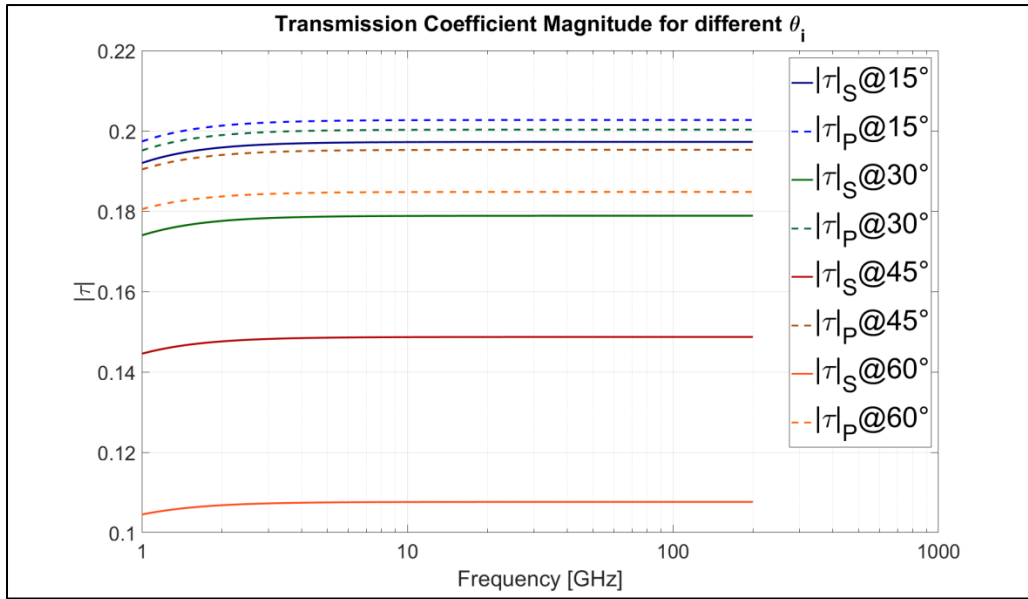


Figure 36. Transmission coefficient values for a FIM model with different angles on incidence.

5.3.2 Frequency Dependent Material (FDM) Model of Water

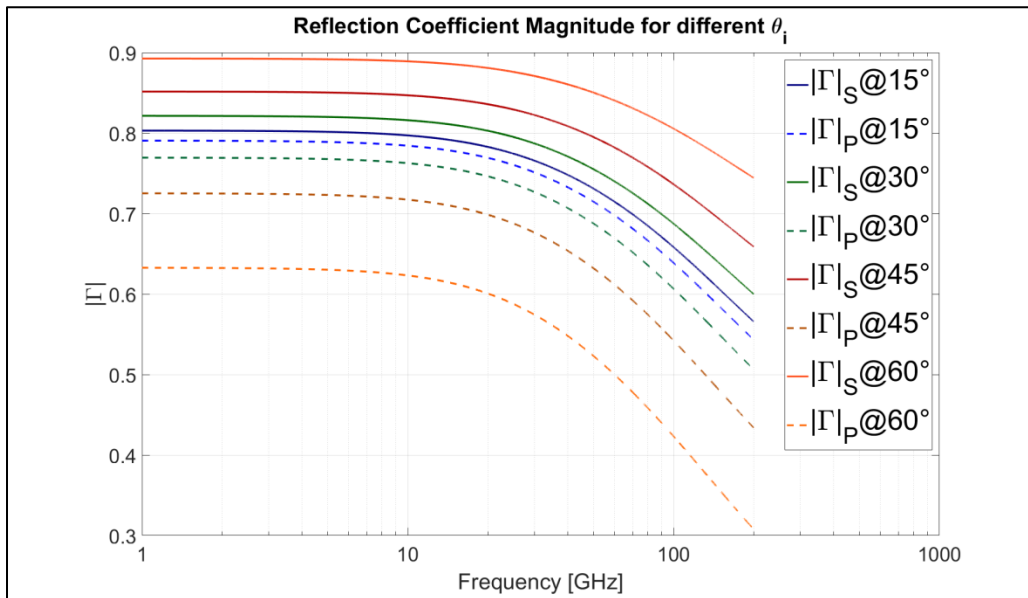


Figure 37. Reflection coefficient values for a FDM model with different angles on incidence.

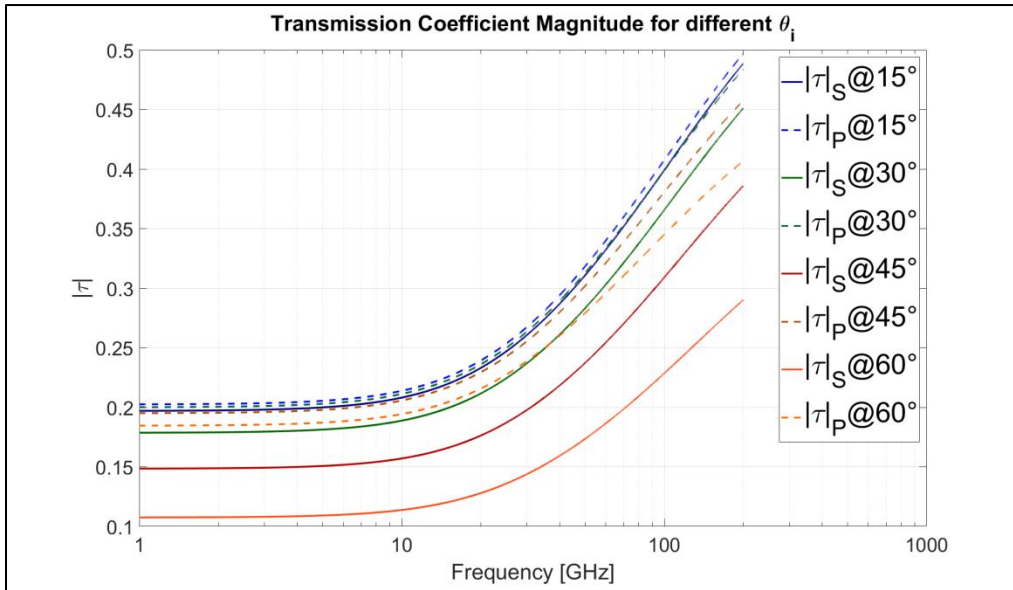


Figure 38. Transmission coefficient values for a FDM model with different angles on incidence.

5.4 Skin Depth of Water

Due to the electrical properties of water, EM fields dissipate at a certain distance once they have been transmitted inside water. How much distance they travel before dissipating is related to the attenuation constant and as we saw in previous subsections, it depends on the model of the material. Both models behave similarly in terms of skin depth but due to the decrease of the electric permittivity of the FDM model, the attenuation decreases slowly in comparison.

Table 17. Skin depth for FDM Model and FIM Model.

Frequency (GHz)	Skin Depth FDM Model (mm)	Skin Depth FIM Model (mm)
1	5.396654074	1.40449438
2	2.706359946	0.97560976
5	1.103630946	0.58582308
10	0.586510264	0.38066235
20	0.346140533	0.23052098
50	0.204750205	0.10414497
100	0.138427464	0.05349204
150	0.106382979	0.03585566

6. Whole-body SAR on a prolate spheroid using physical optics for very high frequencies

Due to the technical limitations of full wave simulations, different methods need to be used to calculate the absorption of energy by biological tissues. One of these methods is to use physical optics to calculate the absorbed power. The basic assumption is that all the energy transmitted into the body (prolate spheroid) is absorbed. This is not a simple assumption, it has been found that for certain geometries the internally reflected rays may be neglected and also from 6 GHz onwards, biological tissue has a depth penetration of 2.6 mm, which makes valid the assumption that all energy transmitted is absorbed [24].

To obtain the whole-body SAR for frequencies higher than 9 GHz, the method developed by [25] was coded in MATLAB. This method requires division of the surface of the prolate spheroid into small patches, calculation of the area of every patch and the definition of a unit-normal vector for each patch. Once these values are obtained, the next step is to find the angle of incidence and transmission of the wave for each patch. Then the transmission coefficients are obtained for each component of the radiation (perpendicular or parallel). Finally the energy transmitted into every patch is calculated and the whole-body SAR is found by summation over all the patches [25].

To implement this method the propagation vector of the incident wave is defined to lie in the XY plane, the formula is given by equation (43) and α is the angle of general incidence of the wave which is defined in figure alpha. The polarizations of the incident wave are represented by unit vector \mathbf{e}_1 and \mathbf{e}_2 , where \mathbf{e}_1 is parallel to the plane defined by the major axis of the prolate spheroid and \mathbf{e}_2 is perpendicular to that plane.

$$\mathbf{a}_k = \sin \alpha \mathbf{a}_x + \cos \alpha \mathbf{a}_z \quad (43)$$

$$\mathbf{e}_1 = -\cos \alpha \mathbf{a}_x + \sin \alpha \mathbf{a}_z \quad (44)$$

$$e_2 = \mathbf{a}_y \quad (45)$$

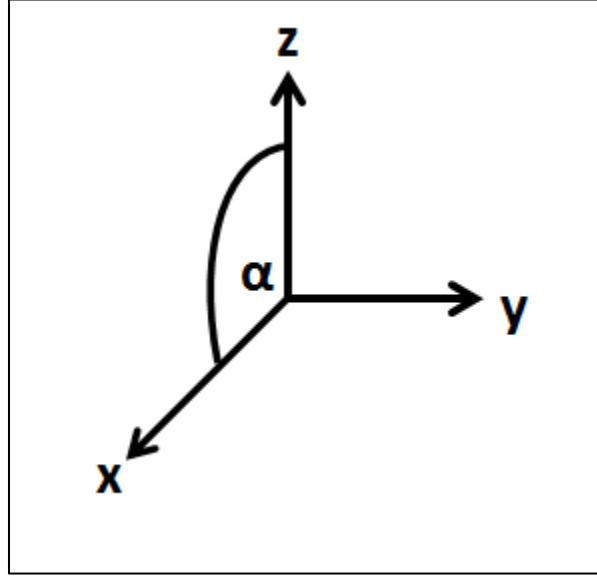


Figure 39. Definition of incident angle alpha for the incident wave.

The angle of incidence for every patch is obtained from equation (46) and once obtained the transmission angle can be found with equation (47).

$$\cos \theta_i = -\mathbf{a}_n \cdot \mathbf{a}_k \quad (46)$$

$$\sin \theta_t = \sin \theta_i / (\varepsilon' - j\varepsilon'')^{1/2} \quad (47)$$

Due to the prolate spheroid geometry, every patch has two reflection coefficients depending on the polarization of the incident wave. Equations (48) and (49) are used to calculate the values of the coefficients for each patch.

$$\Gamma_{\parallel} = \frac{\frac{\cos \theta_t}{(\varepsilon' - j\varepsilon'')^{1/2}} - \cos \theta_i}{\frac{\cos \theta_t}{(\varepsilon' - j\varepsilon'')^{1/2}} + \cos \theta_i} \quad (48)$$

$$\Gamma_{\perp} = \frac{\frac{\sec \theta_t}{(\varepsilon' - j\varepsilon'')^{1/2}} - \sec \theta_i}{\frac{\sec \theta_t}{(\varepsilon' - j\varepsilon'')^{1/2}} + \sec \theta_i} \quad (49)$$

Once the reflection coefficients are obtained, the transmission coefficients for each patch are calculated using equations (50) and (51).

$$\langle S_{t\parallel} \rangle = (1 - |\Gamma_{\parallel}|^2) \quad (50)$$

$$\langle S_{t\perp} \rangle = (1 - |\Gamma_{\perp}|^2) \quad (51)$$

These coefficients must be implemented in the proper manner, the incident electric field must be broken up into two components for each subarea: one parallel to the plane of incidence and one perpendicular to this plane. A method of finding these components of the incident electric field is to define a unit vector perpendicular to the plane of incidence on each patch and then to find components of the incident wave's polarization vector, which are parallel and perpendicular to this vector. A unit vector perpendicular to the plane of incidence is found in equation (52) [24].

$$\mathbf{a}_m = -[(\mathbf{a}_n \times \mathbf{a}_k) / \sin \theta_i] \quad (52)$$

Once this vector is obtained for each patch, equation (53) can be used to obtain the power absorbed from each patch for the parallel incident wave. Where S_i is the incident power density and A_P is the projected area of each patch which can be found using equation (55). For \mathbf{e}_2 the formula used is found in equation (54).

$$P_1 = S_i A_P \left\{ (\mathbf{e}_1 \cdot \mathbf{a}_m)^2 (1 - |\Gamma_{\perp}|^2) + [1 - (\mathbf{e}_1 \cdot \mathbf{a}_m)^2] (1 - |\Gamma_{\parallel}|^2) \right\} \quad (53)$$

$$P_2 = S_i A_P \left\{ (\mathbf{e}_2 \cdot \mathbf{a}_m)^2 (1 - |\Gamma_{\perp}|^2) + [1 - (\mathbf{e}_2 \cdot \mathbf{a}_m)^2] (1 - |\Gamma_{\parallel}|^2) \right\} \quad (54)$$

$$A_P = A_{Patch} * \cos \theta_i \quad (55)$$

6.2 EHK Polarization

In this section the results of the physical optics approach are presented for the E polarizations. To get a better understanding of the results, the whole-body SAR obtained using CST is put against the values obtained with the proposed methodology. There is a seemingly good correspondence between both measurements. Where the full-wave simulation reaches its limit, the optical approach can be seen as a continuation of the tendency marked by the frequency range from 5 GHz to 9 GHz.

In figure 40, the material used is water modelled as a FI material, while in figure 41 water is modelled as a FD material. While there are no big differences when plotted in the range of interest, some differences in magnitude can be appreciated on figure 42.

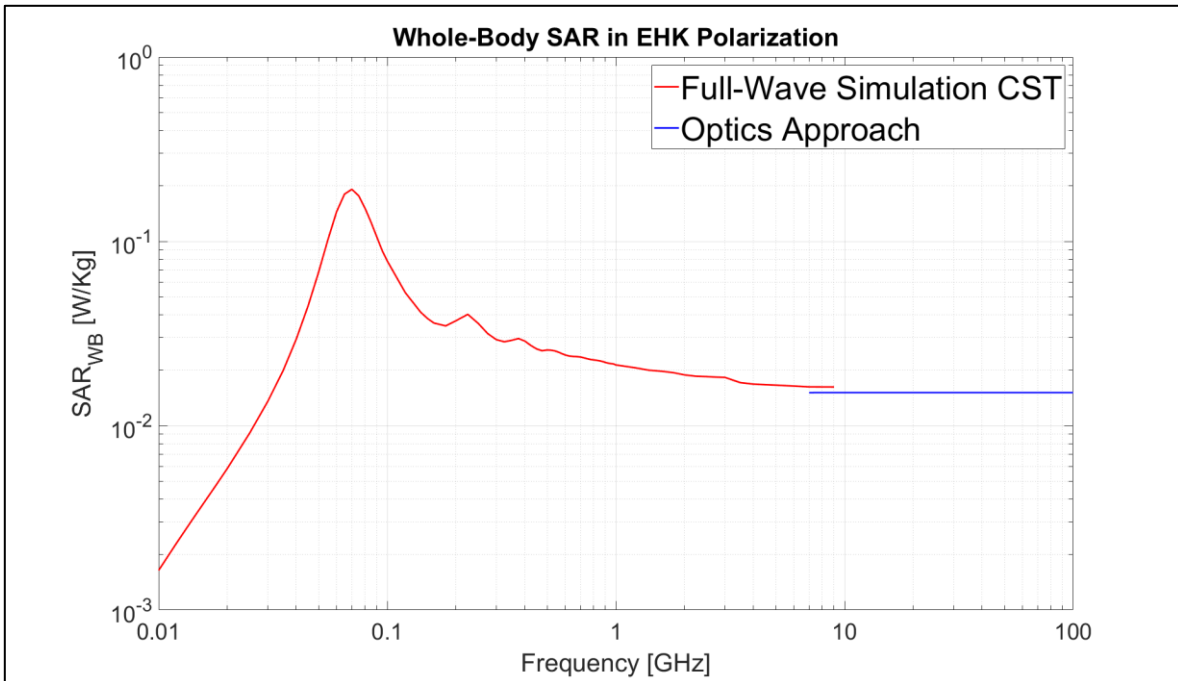


Figure 40. Whole-body SAR for E polarization up to 100 GHz using a FIM model.

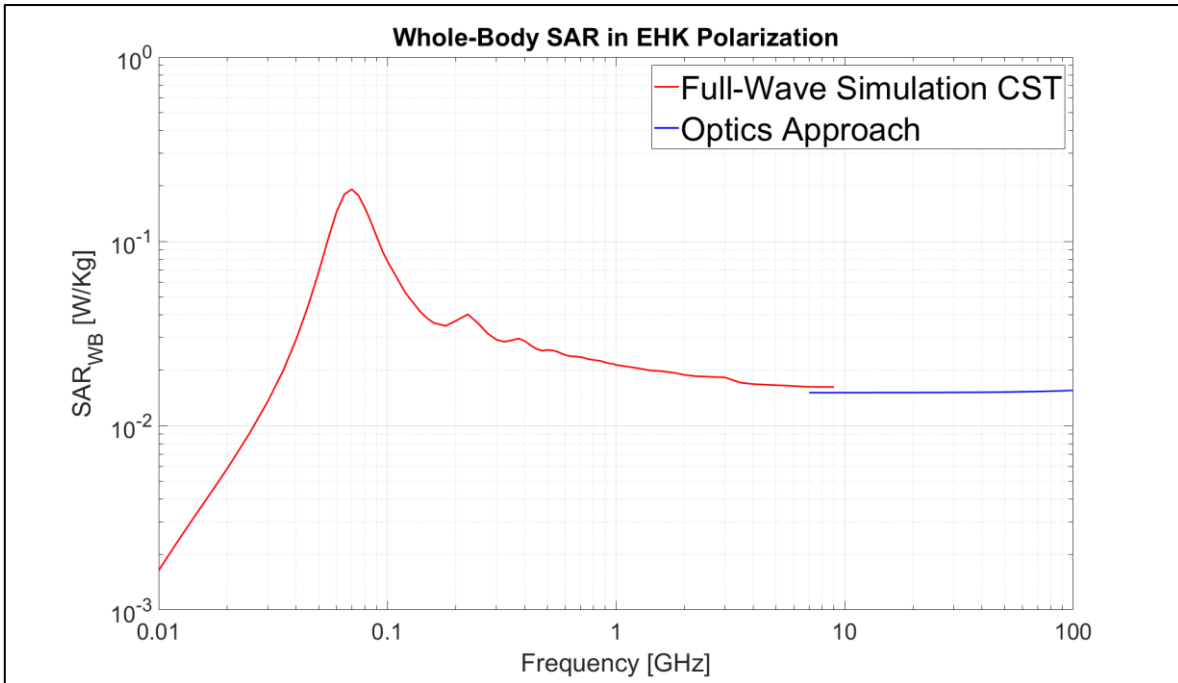


Figure 41. Whole-body SAR for E polarization up to 100 GHz using a FDM model.

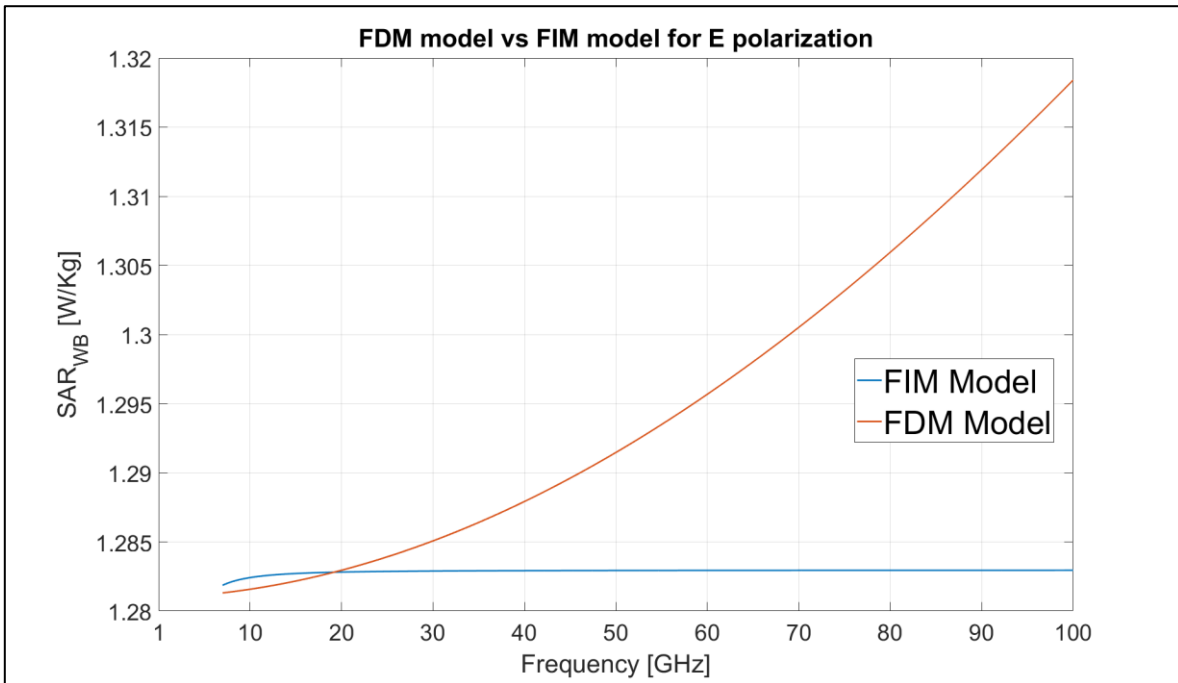


Figure 42. FDM Model vs FIM Model for E polarization.

6.3 HEK Polarization

Similar to EHK polarization, EHK exhibits a good correspondence between the full-wave simulations and the optical approach. Again there seems to be a “saturation” value achieved in the higher frequencies which can be addressed to the full absorption assumption made by the methodology [24].

In similar fashion to EHK polarization, there are some differences in the results that are not quite visible when the full spectrum is presented. Figure 43 showcases the use of a FIM model of water and figure 44 a FDM model. Their differences can be seen in figure 45 and while they are quite small we can see that they really exist.

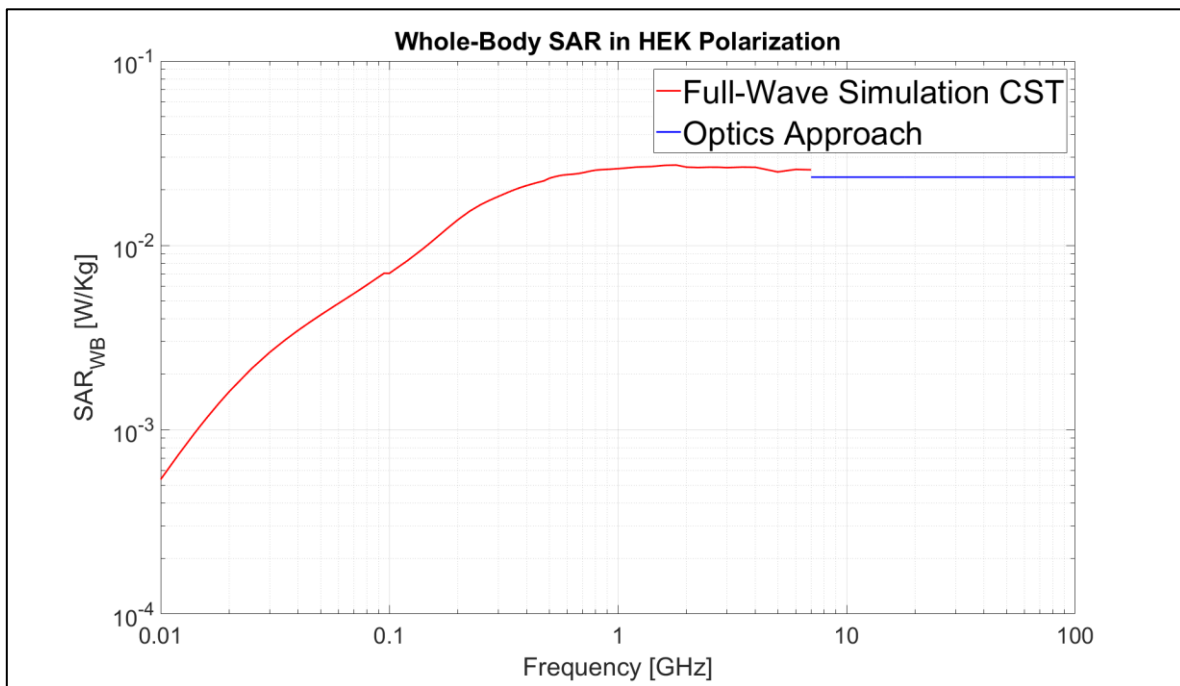


Figure 43. Whole-body SAR for H polarization up to 100 GHz using a FIM model.

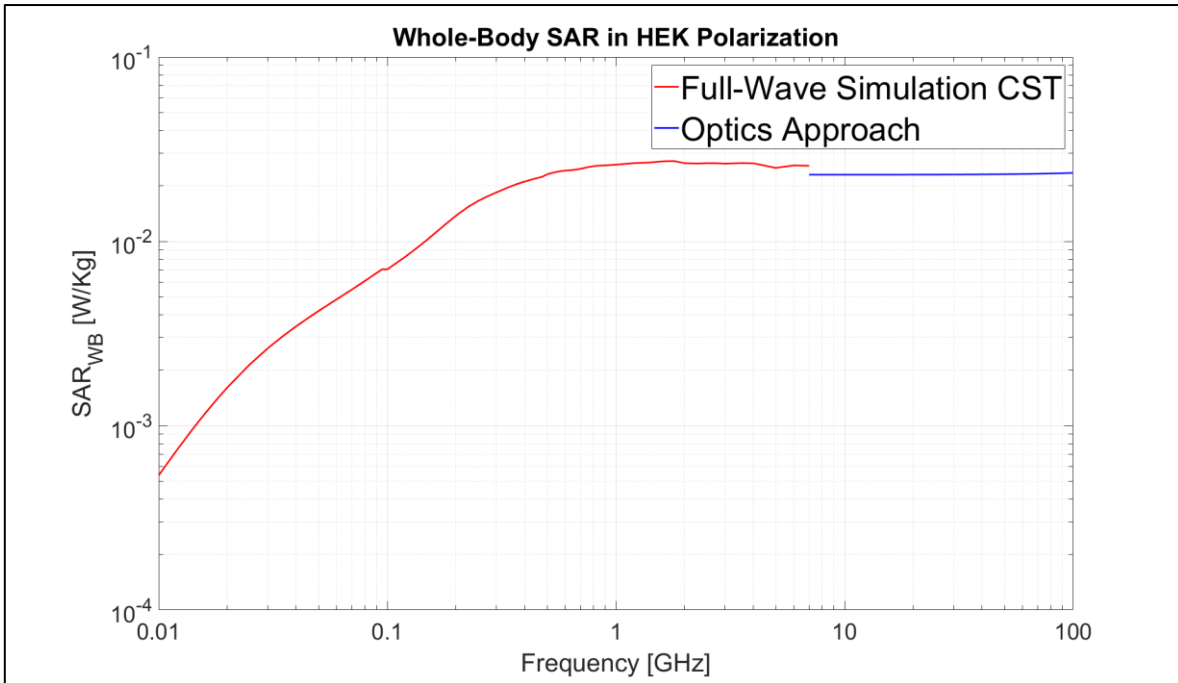


Figure 44. Whole-body SAR for H polarization up to 100 GHz using a FDM model.

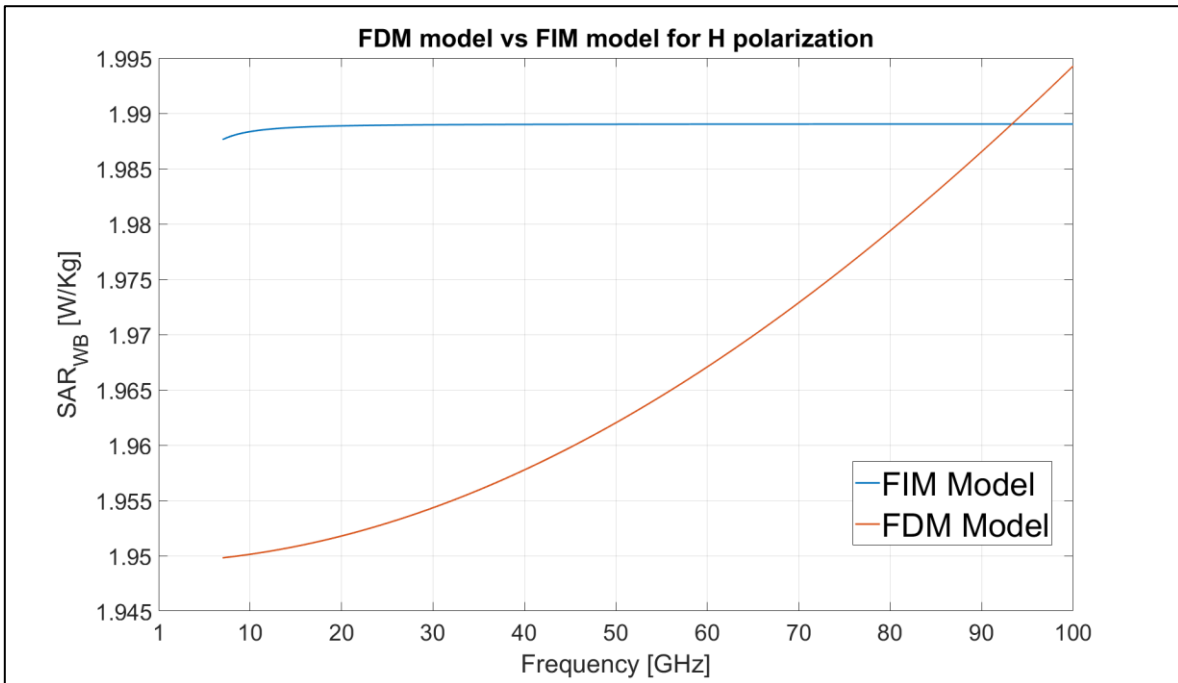


Figure 45. FDM Model vs FIM Model for H polarization.

6.4 KEH Polarization

Finally, in KEH polarization the methodology seems to fail due to the big differences between both approaches. There is an important observation to be made. In figure 5 there is a full characterization of the whole-body SAR when the plane wave is in K polarization. The reason behind this complete curve is that values were assumed to connect the low frequency end to the high frequency end, so in reality there is no real knowledge of the behavior of K polarization in a wide frequency range.

Here, the behavior up to 9 GHz was successfully described using full-wave simulators, which increased some of the blank space filled in figure 5. Still, there is a big difference for frequencies higher than 9 GHz as shown by the optical approach.

One particular reason for this difference is that the physical optics approach works best when there is little to no curvature of the geometry of interest, so while E and H polarizations have an almost “planar” surface due to the relative size of the wavelength to the size of the body. In the case of K polarization the front on which the wave radiates has a surface with a pretty high curvature. This could render the approach for this polarization useless.

Another difference is that while E and H polarization waves travel through a small length of the prolate spheroid, K polarization travels through the longer part of it. This could also make some difference on the utility of the approach. Finally, as with other polarizations, there are differences when water is modelled as frequency dependent or frequency independent, those differences can be seen on figure 48.

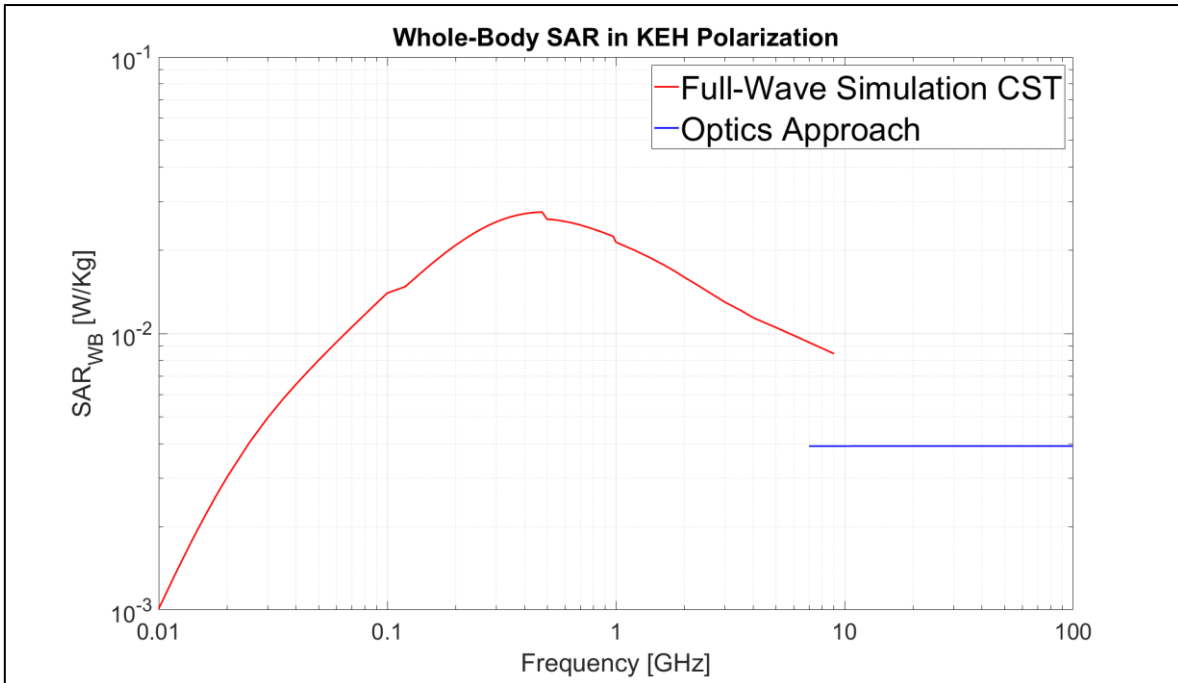


Figure 46. Whole-body SAR for K polarization up to 100 GHz using a FIM model.

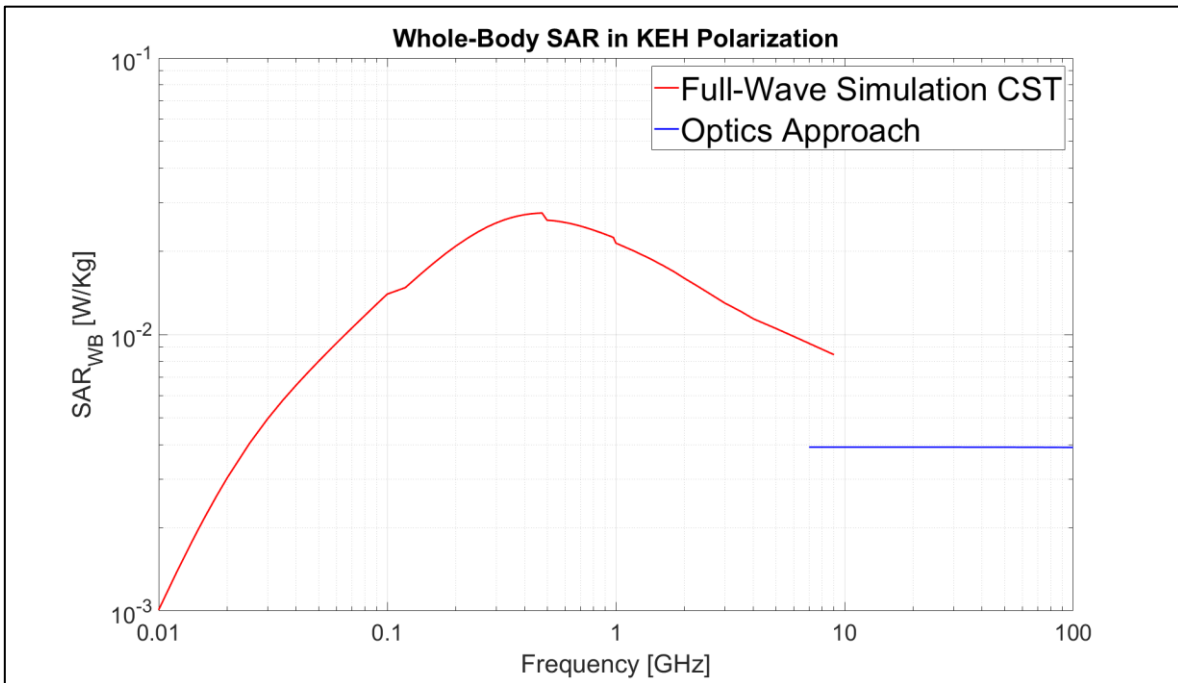


Figure 47. Whole-body SAR for K polarization up to 100 GHz using a FDM model.

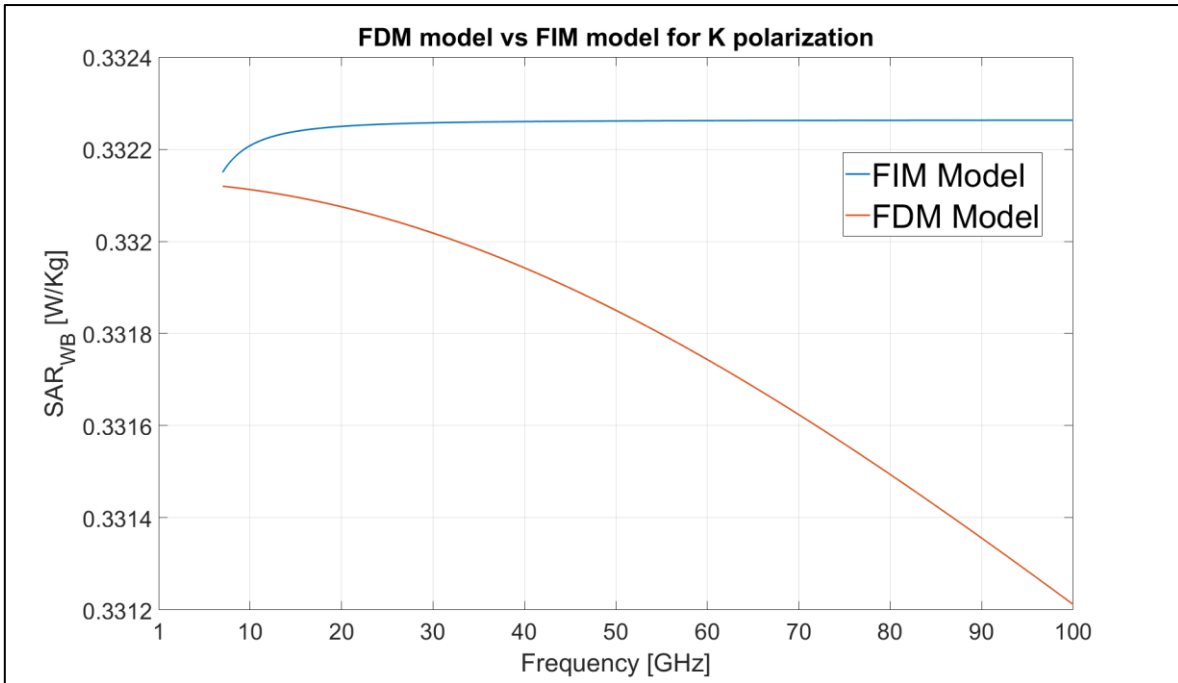


Figure 48. FDM Model vs FIM Model for K polarization.

6.5 Full spectrum of whole-body SAR in terms on different wave polarizations

In this final subsection, the 3 polarizations are shown against each other for the full range of interest from 10 MHz to a 100 GHz. There is an almost equal correspondence to that of figure 5, where its differences arise from the different values chosen and in case of K polarization to the limitations of the optics approach.

Figure 49 shows the use of water modelled as a FI material for the optics approach and figure 50 shows water modelled as a FD material for the optics approach.

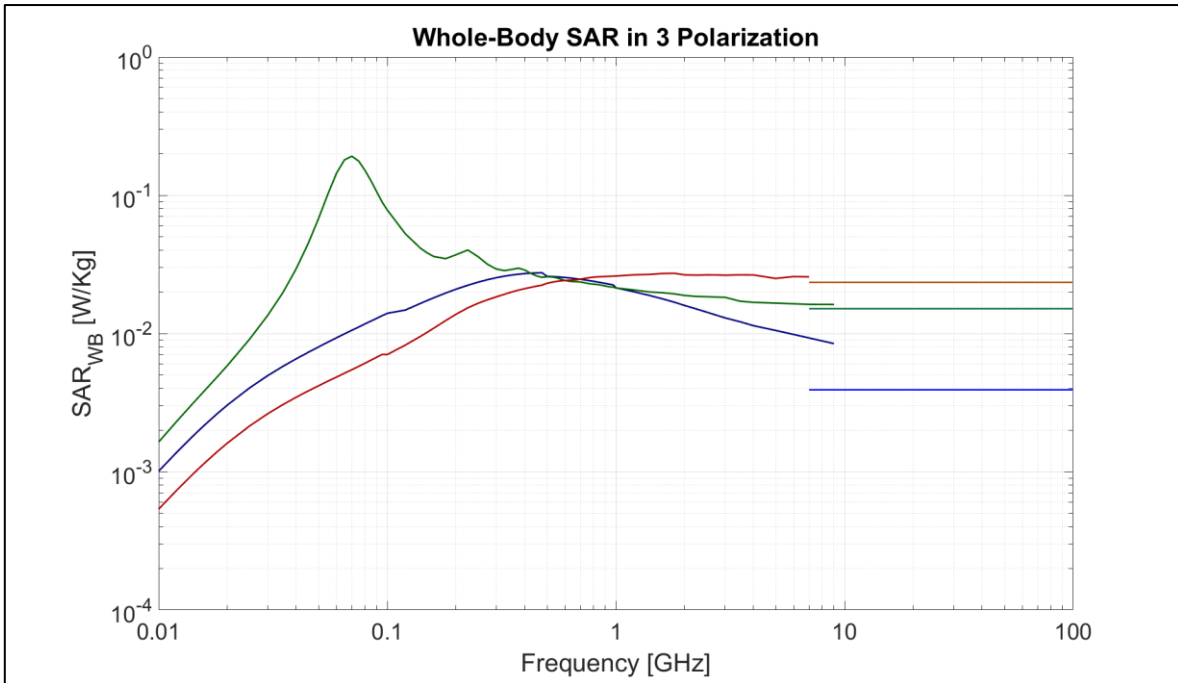


Figure 49. Whole-body SAR for 3 polarizations up to 100 GHz using a FIM model.

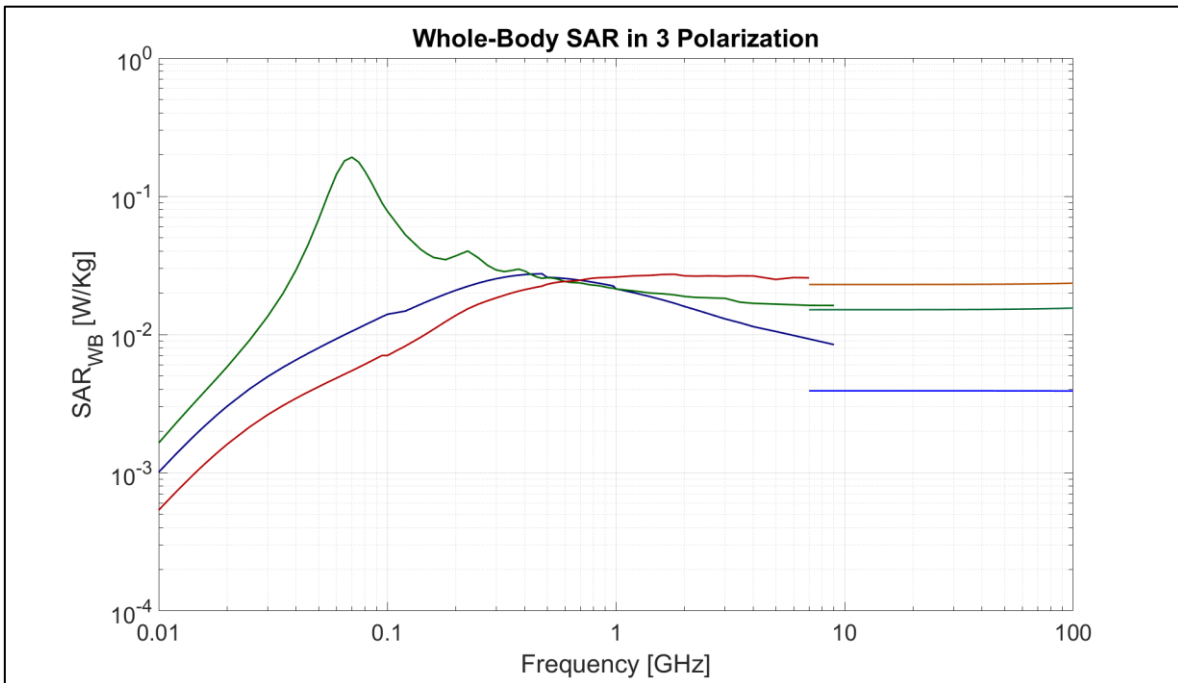


Figure 50. Whole-body SAR for 3 polarizations up to 100 GHz using a FDM model.

7. Conclusions

A full methodology to calculate the whole-body SAR for a prolate spheroid using different wave polarizations has been developed. However, this method is far from perfect and only can be used with the aforementioned geometry. Also, MATLAB scripts were developed to model a 1D problem of reflection to study the behavior of water as a material.

Full wave simulations for big electric bodies are still a resource demanding process. Even with the technological advances in computing power and the optimization of numerical methods for CEM computations, this kind of problems are very difficult to simulate in frequencies higher than 10 GHz. The number of elements, be it mesh cell or unknowns, needed to compute at these high frequencies scales so greatly that there is no way of performing this simulation without the help of super computers. It must be noted that these limitations are for a simple geometrical model with a homogeneous material, if simulations for more complex bodies were desired, the limitations would start in lower frequencies.

Another important aspect of these simulations is that even though using MoM to solve the problem proves to be faster, the memory needed to sustain the high frequency simulations is much bigger than the one needed for a program like CST. This can be seen in the limits reached by both methods, where even if the RAM resources to run the CONCEPT-II simulations were bigger than the ones for CST, in the end, CST reached a higher frequency limit in the simulations. It is also important to note that CONCEPT doesn't have all the options in terms of symmetry and for this reason the H polarization is heavily affected in terms of range in comparison to CST where all 3 polarizations reached the same frequency limit. Finally, due to the disadvantages of MoM with dielectric modeling, the calculation of EM fields starts to fail for certain polarizations albeit being able to calculate the surface currents needed to compute the solution.

Once the full wave method limit is reached, the physical optics approach is one answer to the problem of the computational limitations presented in the simulations. Thanks to behavior described by the material definition like skin effect, this approach is used to give an approximation of the characteristics of radiation in very high frequencies. The formulation of the solution is quick, efficient and gives a valuable approximation of the behavior expected by the theory. Unfortunately, this formulation is a solution specific to the geometry of interest and limits the application of this formulation.

In regard to the material modeling, differences are found, not only with the propagation direction of the incident wave, but also the frequency dependence of the material. The perpendicular incidence gives us an understanding of the material variations in terms of frequency but it is limited to very unique scenarios. For that reason, the general incidence scenario helps us understand how radiation behaves in a broader sense, which can be applied to the original model of interest.

8. Recommendations

The use of more computing power is still a valid recommendation to push the simulations limit to a new maximum frequency; however, is the most difficult to implement due to economic constraints. Changes in the prolate spheroid dimensions can be used to study the effects of other human body types like children or babies. Also, changing the prolate spheroid for an ellipsoid can give a better insight of the behavior of EM radiation on humans due to the similar cross-section and the use of 6 wave polarizations instead of 3.

Further analyses can be performed using the prolate spheroid; for example, two spheroids next to each other can be used to simulate the effect of a person shielding another from EM radiation. Another line of research would be to use the spheroid with a thin sheet covering it to simulate clothing, which is a variable often forgot in this kind of simulations. These simulations would apply in the realm of full-wave simulators and not with the physical optics approach.

It is also recommended to study other methodologies in terms of the high frequency range (10 GHz – 100 GHz) due to the geometrical limitations of the physical optics approach. If another method can be developed without a geometrical dependency it could help get better results of the high frequency effects for more complex models like a full human body.

In terms of mesh density of the models, an optimal value should be found in full-wave simulators in terms of the tradeoff between accuracy of the results and speed of the simulations. Finally, the use of a full body will always be demanding for simulations, for this reason a localized study is an option to speed up simulation times and also to study the SAR in more specific areas.

9. References

- [1] C. H. Durney, «Radiofrequency Radiation Dosimetry Handbook,» Utah, 1986.
- [2] A. Hirata, S.-i. Matsuyama y T. Shiozawa, «Temperature Rises in the Human Eye Exposed to EM Waves in the Frequency Range 0.6-6 GHz,» IEEE Transactions on Electromagnetic Compability, vol. 42, n° 4, pp. 386-393, 2000.
- [3] D. A. Hill, «Effect of Separation From Ground on Human Whole-Body RF Absorption Rates,» IEEE Transactions on Microwave Theory and Techniques, Vols. %1 de %2MTT-32, n° 8, pp. 772-778, 1984.
- [4] P. Bernardi, M. Cavagnaro y S. Pisa, «Specific Absorption Rate and Temperature Elevation in a Subject Exposed in the Far-Field of Radio-Frequency Sources Operating in the 10-900-MHz Range,» IEEE Transactions on Biomedical Engineering, vol. 50, n° 3, pp. 295-304, 2003.
- [5] A. G. Canseven y N. Seyhan, «Ellipsoid Models for Human and Guinea Pigs Exposed to Magnetic Fields,» pp. 1227-1231, 2003.
- [6] E. Cocherova, J. Surda, O. Ondracek y V. Stofanik, «RF Field Orientation Influence on the Specific Absorption Rate in a Biological Object,» 2008.
- [7] E. Cocherova, J. Surda, J. Pucik y V. Stofanik, «Dependence of the RF Field Absorption on the Human Body Dimensions,» 2009.
- [8] A. Hirata, O. Fujiwara, T. Nagaoka y S. Watanabe, «Estimation of Whole-Body Average SAR in Human Models Due to Plane-Wave Exposure at Resonance Frequency,» IEEE Transactions on Electromagnetic Compatibility, vol. 52, n° 1, pp. 41-48, 2010.
- [9] E. Conil, A. Hadjem, A. Gati, M.-F. Wong y J. Wiart, «Influence of Plane-Wave Incidence Angle on Whole Body and Local Exposure at 2100 MHz,» IEEE Transactions on Electromagnetic Compatibility, vol. 53, n° 1, pp. 48-52, 2011.
- [10] N. Chahat, M. Zhadobov, L. Le Coq, S. I. Alekseev y R. Sauleau, «Characterization of the Interactions Between a 60-GHz Antenna and the Human Body in an Off-Body Scenario,» IEEE Transactions on Antennas and Propagation, vol. 60, n° 12, pp. 5958-5965, 2012.
- [11] M. Lu y X.-Y. Wu, «Study of Specific Absorption Rate (SAR) Induced In Human Endocrine Glands For Using Mobile Phones,» de 7th Asia Pacific International Symposium on Electromagnetic Compatibility, 2016.
- [12] Z. Pšenáková y M. Beňová, «Evaluation of SAR (Specific Absorption Rate) in multilayer structure of biological tissues near ear with cochlear implant,» de 2017 18th International Conference on Computational Problems of Electrical Engineering (CPEE), Czech Republic, 2017.
- [13] P. Dimbylow y W. Bolch, «Whole-body-averaged SAR from 50 MHz to 4 GHz in the University of Florida child voxel phantoms,» Physics in Medicine and Biology, vol. 52, pp. 6639-6649, 2007.

- [14] M. M. Búrdalo, A. Martín, M. Anguiano y R. Villar, «Comparison of FDTD-calculated specific absorption rate in adults and children when using a mobile phone at 900 and 1800 MHz,» *Physics in Medicine and Biology*, vol. 49, pp. 345-354, 2004.
- [15] T. Nagaoka, E. Kunieda y S. Watanabe, «Proportion-corrected scaled voxel models for Japanese children and their application to the numerical dosimetry of specific absorption rate for frequencies from 30 MHz to 3 GHz,» *Physics in Medicine and Biology*, vol. 53, pp. 6695-6711, 2008.
- [16] P. J. Dimbylow y O. P. Gandhi, «Finite-difference time-domain calculations of SAR in a realistic heterogeneous model of the head for plane-wave exposure from 600 MHz to 3 GHz,» *Physics in Medicine and Biology*, vol. 36, nº 8, pp. 1075-1089, 1991.
- [17] J. A. Carballo-Madrigal, H.-D. Brüns, R. Rímolo-Donadio y C. Schuster, «Full-Wave Simulation of Body Absorption due to Radiated Fields at GHz Frequencies,» *Tecnología en Marcha*.
- [18] A. Christ, A. Klingenbock, T. Samaras, C. Goiceanu and N. Kuster, "The dependence of electromagnetic far-field absorption on body tissue composition in the frequency range from 300 MHz to 6 GHz," in *IEEE Transactions on Microwave Theory and Techniques*, vol. 54, no. 5, pp. 2188-2195, May 2006.
- [19] Popović, M., Han, Q. & Kanj, H. *Environmentalist* (2005) 25: 233. <https://doi.org/10.1007/s10669-005-4288-4>
- [20] C. Lazarescu, I. Nica and V. David, "SAR in human head due to mobile phone exposure," 2011 E-Health and Bioengineering Conference (EHB), Iasi, 2011, pp. 1-4.
- [21] C. Furse, D. A. Christensen & C. H. Durney. (2009). "Basic Introduction to Bioelectromagnetics". CRC Press.
- [22] D. M. Pozar, *Microwave engineering*. New York, NY: Wiley, 1998.
- [23] H.J. Liebe, G.A. Hufford & T. Manabe. (1991)" A model for the complex permittivity of water at frequencies below 1 THz"
- [24] G.I Rowlandson & P.W Barber (1979) "Absorption of higher-frequency RF energy by biological models: Calculations based on geometrical optics"